

# Motion Planning for Multirotor Aerial Vehicles in Plan-based Control Paradigm: a Review

Geesara Kulathunga<sup>a</sup>, Alexandr Klimchik<sup>a</sup>

<sup>a</sup>*Center for Technologies in Robotics and Mechatronics Components, Innopolis University, Russia*

---

## Abstract

In general, optimal motion planning can be performed both locally and globally. In such a planning, the choice in favour of either local or global planning technique mainly depends on whether the environmental conditions are dynamic or static. Hence, the most adequate choice is to use local planning or local planning alongside global planning. When designing optimal motion planning both local and global, the key metrics to bear in mind are execution time, asymptotic optimality, and quick reaction to dynamic obstacles. Such planning approaches can address the aforesaid target metrics more efficiently compared to other approaches such as path planning followed by smoothing. Thus, the foremost objective of this study is to analyse related literature in order to understand how the motion planning, especially trajectory planning, problem is formulated, when being applied for generating optimal trajectories in real-time for Multirotor Aerial Vehicles (MAVs), impacts the listed metrics. As a result of the research, the trajectory planning problem was broken down into a set of subproblems, and the lists of methods for addressing each of the problems were identified and described in detail. Subsequently, the most prominent results from 2010 to 2022 were summarized and presented in the form of a timeline.

*Keywords:* MAVs, B-Spline, Minimum-snap, Model Predictive Control (MPC), Nonlinear Model Predictive Control (NMPC), Linear Quadratic Regulator (LQR), Differential Dynamic Programming (DDP), Optimal Control Problem (OCP), Quadratic Programming (QP), Safe Flight Corridor (SFC), Gradient-based Trajectory Optimization (GTO), Truncated Signed

### List of Abbreviations

	<b>BFGS</b>	Broyden—Fletcher—Goldfarb—Shanno.
	<b>CBFs</b>	Control Barrier Functions.
5	<b>CHOMP</b>	Covariant Hamiltonian Optimization for Motion Planning.
	<b>CMPPC</b>	Corridor-based Model Predictive Contouring Control.
	<b>DDP</b>	Differential Dynamic Programming.
	<b>EO</b>	Elastic Optimization.
	<b>ESDF</b>	Euclidean Signed Distance Field.
10	<b>GTC</b>	Geometric Tracking Control.
	<b>GTO</b>	Gradient-based Trajectory Optimization.
	<b>iLQR</b>	Iterative Linear Quadratic Regulator.
	<b>IRIS</b>	Iterative Regional Inflation by Semi-definite Programming.
	<b>JPS</b>	Jump Point Search.
15	<b>KF</b>	Kalman Filter.
	<b>LQG</b>	Linear Quadratic Gaussian.
	<b>LQR</b>	Linear Quadratic Regulator.
	<b>LTl</b>	Linear Time Invariant.
	<b>MAV</b>	Multirotor Aerial Vehicle.
20	<b>MAVs</b>	Multirotor Aerial Vehicles.
	<b>MHE</b>	Model Horizon Estimation.
	<b>MIQP</b>	Mixed Integer Quadratic Programming.
	<b>MPC</b>	Model Predictive Control.
	<b>MPCC</b>	Mathematical Program with Complementarity Constraints.
25	<b>NLP</b>	Nonlinear Programming.
	<b>NMPC</b>	Nonlinear Model Predictive Control.
	<b>OCP</b>	Optimal Control Problem.
	<b>OCPs</b>	Optimal Control Problems.

	<b>PGO</b>	Path-guided Optimization.
30	<b>PRM</b>	Probabilistic Road Map.
	<b>QCQP</b>	Quadratically Constrained Quadratic Programming.
	<b>QP</b>	Quadratic Programming.
	<b>RHC</b>	Receding Horizon Control.
	<b>RRG</b>	Rapidly-exploring Random Graph.
35	<b>SDDM</b>	State-dependant Distance Metric.
	<b>SFC</b>	Safe Flight Corridor.
	<b>SQP</b>	Sequential Quadratic Programming.
	<b>TOPP</b>	Time-Optimal Parameterization of a given Path.
	<b>TSDF</b>	Truncated Signed Distance Field.
40	<b>UAV</b>	Unmanned Aerial Vehicle.
	<b>UAVs</b>	Unmanned Aerial Vehicles.

## 1. Introduction

Adroit motion planning of flying little creatures, such as birds and butterflies, is an extraordinarily demanding task for several reasons, including aggressive maneuver. An example of such high-speed maneuver need is one in particularly tight spots where the environment is obstacle-rich. Researchers have been trying to replicate similar maneuvers using two different types of aerial vehicles: conventional and unconventional. In this research we deal with conventional areal vehicles, for instance, Unmanned Aerial Vehicles (UAVs), Multirotor Aerial Vehicles (MAVs), etc. Recent progression in computation capabilities and embedded sensing has been boosting the procedure of mimicking natural flying animals; this advancement has enabled plenty of new opportunities in diverse fields: inspection, autonomous transportation, logistics, delivery, areal photography, post-disaster and medical services. Yet optimal motion planning remains a crucial task in all the fields listed above. In optimal motion planning, the environmental reasoning can not be predictable since environmental conditions

change rapidly. Hence, there are various challenges to be addressed to obtain highly efficient and optimal motion planning. In this paper, we mainly focus on how researchers have been addressing these challenges in optimal motion  
60 planning to obtain robust navigation in various domains for MAVs.

In most of the foregoing applications, the environment is entirely or partially unexplored. Furthermore, unpredictable events can occur at any time due for numerous reasons. Thus, to tackle those unexpected problems in real time, a fast and accurate optimal motion planning technique is required. In general,  
65 the optimal motion planning problem is divided into a few subcategories: path planning followed by smoothing, kinodynamic search-based trajectory generation, and motion primitive-based approaches. Among them, plan-based control approaches are the most widely used and efficient way to address the considered problem compared to the other two approaches. Plenty of plan-based control  
70 strategies have been proposed throughout the recent decade, showing promising results; this is one of the key motivating factors for reviewing plan-based control, especially for industrial MAVs. Most of the industrial MAVs such as quadrotors have their low-level controllers, for example, PX4 [1], DJI [2], that can be operated independently irrespective of high-level execution commands.  
75 Moreover, such controllers reduce the overhead and complexity for developing high-level planning algorithms due to their independence. In other words, the same planner can be deployed on different firmware by implementing an interface between a high-level planner and a low-level controller. Thus, we narrowed down our study to considering only plan-based control approaches (Fig. 1), particularly  
80 in application to industrial MAVs.

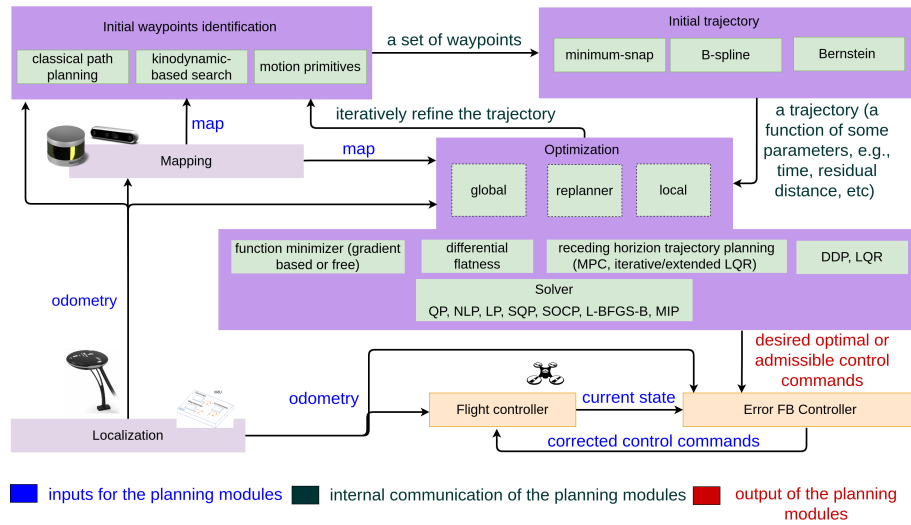
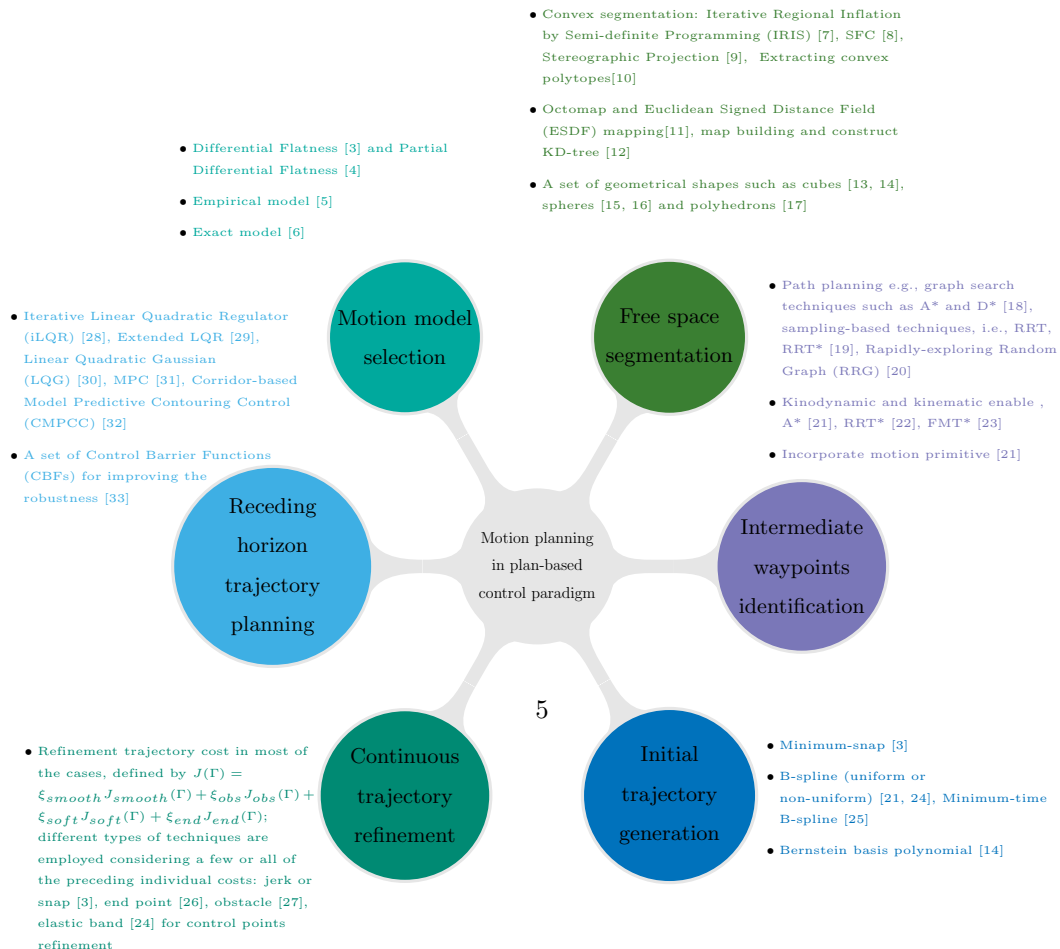


Figure 1: The overview of plan-based control paradigm in the context of trajectory planning problem formulation. There are various ways to formulate the trajectory planning problem, each of which consists of a set of sub-modules (green color boxes) depending on the problem behaviour



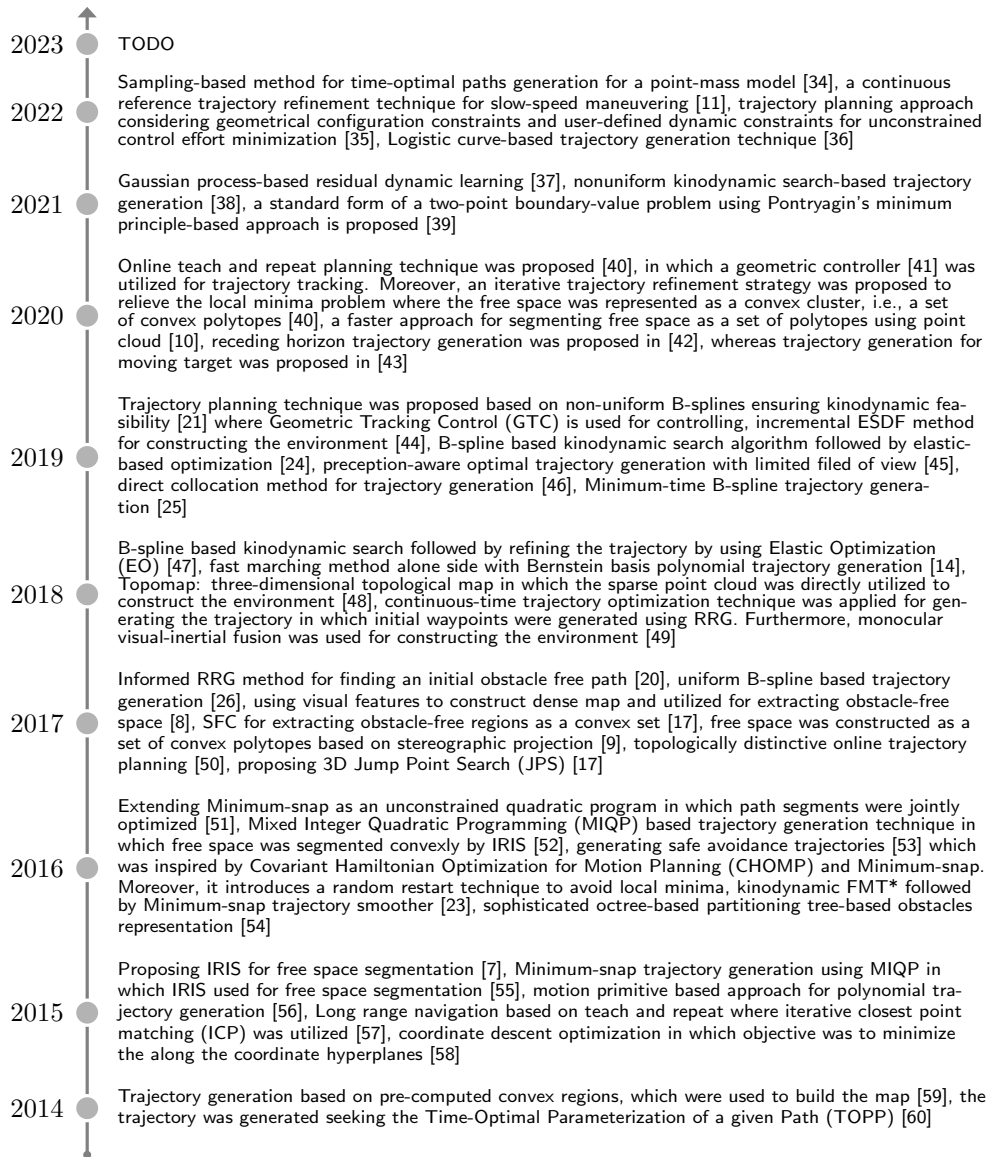


Figure 3: The most prominent related research outcomes which led the success of the trajectory planning for MAVs in the last decade

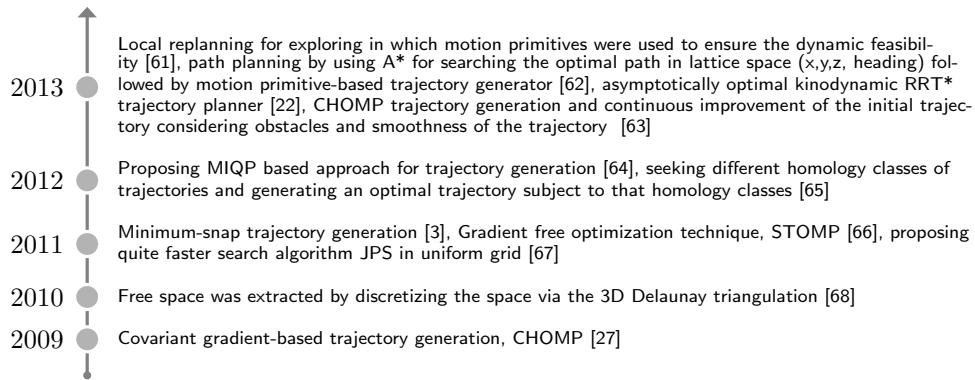


Figure 4: The most prominent related research outcomes which led the success of the trajectory planning for MAVs in the last decade

The main limitation of MAVs is low flight time. Hence, a MAV should be capable of executing robust, agile, aggressive maneuver while ensuring dynamic feasibility and guaranteeing smoothness of the trajectory in low flight time. Furthermore, trajectory plotting should be performed within an obstacle-free zone at high-speed to handle a given mission effectively. Such behaviour is imposed by adhering to a set of constraints. If and only if the constraints are incorporated appropriately, desired needs can be fulfilled. Obtaining the right constraints at the right moment and applying appropriate control sequences to improve motion quality is the key objective of any plan-based control approach. Yet the procedure of obtaining such right constraints is an open research problem due to its complexity and numerous other challenges that should be handled simultaneously. For example, Multirotor Aerial Vehicle (MAV) has been widely employed in video-making related fields in recent years, cinematographic aerial shooting being one of the popular areas of interest during the last five years. In such shooting, generating smooth, obstacle-free trajectories is the main challenge. Besides, various other challenges exist, and most of them are application-specific. In this work, we examine the most common problems related to trajectory planning applications in the paradigm of plan-based control,

and how researchers have been alleviating those problems by proposing compelling solutions.

In optimal trajectory planning, trajectory generation and controlling the MAV are strongly interconnected. For MAVs, the trajectory generation process is relatively easy due to the dynamic properties of the MAVs. When dynamic obstacles are incorporated, the trajectory has to be refined at a high rate in order to keep a smooth maneuver despite increased computational demands. Moreover, understanding close-in obstacles' positions relative to the MAV is crucial for making decisions in real-time; this arises a new challenge: the one of the rapidity and accuracy of relative environment reconstruction, which essentially is how obstacles constraints are added to the problem formulation. Yet another challenge is of the impact of the obstacles and constraints on the smoothness and dynamic feasibility of the generated trajectory. After conducting an extensive literature review on the topic of trajectory planning for MAVs, we were able to isolate basic building blocks that are essential for optimal motion planning as shown in Fig. 2. Each of the primary components plays a key role in the process of trajectory generation. The rest of the paper focuses on understanding how those building blocks are interconnected in solving trajectory planning problems.

The rest of the paper is organized as follows: section 2 explains what type of motion model is likely to be suitable for defining the dynamics of MAV based on the chosen trajectory generation technique. Then, state-of-the-art techniques on how to find initial tentative waypoints for trajectory generation is explained in section 3. Section 4 presents an extensive review on initial trajectory generation techniques. Section 5 explains how free space is extracted and incorporated into trajectory planning. The trajectory refinement process is explained in section 6. Horizon-based trajectory planning techniques are described in section 7. Various solvers which can be used to solve the optimization problem are detailed under section 8.



## 2. Motion Model Selection

Exact model, empirical model and differential flatness are the main tech-  
 130 niques that can be employed for selecting the most appropriate motion model  
 for a specified application. The appropriate motion model selection procedure  
 varies depending on the problem formulation. For example, planning followed  
 by controlling approaches does not necessarily have an exact motion model  
 mainly due to high computational demands. In such scenarios, an empirical  
 135 motion model is sufficient for planning, since a dedicated controller is utilized  
 for controlling the quadrotor.

### 2.1. Exact Model

In general, MAV dynamics is described by 12-DOF. However, in planning  
 followed by high-level controlling approaches, it is not required to define an  
 140 actual motion model for planning, since a high-level controller consists of a  
 fully-fledged quadrotor motion model. In most circumstances, the planner is  
 comprised of approximated quadrotor dynamics; this is due to computational  
 complexity, which is not adequate for real-time onboard processing. Hence,  
 the motion model selection process depends on the approach that formulates  
 145 needs. In [6], the researchers proposed a 12-DOF motion model whose state  
 vector is defined by  $\mathbf{x} = [\mathbf{p}^\top, \mathbf{v}^\top, \psi^\top, \omega^\top]$ , where  $\psi$ ,  $\mathbf{p}$ ,  $\mathbf{v}$  and  $\omega$  stand for  
 orientation (rad), position (m), velocity (m/s) and angular velocity (rad/s)  
 in  $\mathbb{R}^3$ , respectively. The system input or total thrust that is applied for each  
 of the motors is given by  $\mathbf{f} = [f_1, f_2, f_3, f_4]^T$  (N). System dynamics is deter-  
 150 mined as  $\dot{\mathbf{x}} = [\dot{\mathbf{p}}^\top, \dot{\mathbf{v}}^\top, \dot{\psi}^\top, \dot{\omega}^\top]$ , where  $\dot{\mathbf{p}} = \mathbf{v}$ ,  $\dot{\mathbf{v}} = -g \cdot \mathbf{e}_z + \frac{(\mathbf{f} \cdot \exp[\psi] \cdot \mathbf{e}_z - k_v \cdot \mathbf{v})}{m}$ ,  
 $\dot{\psi} = \omega + \frac{1}{2}[\psi] \cdot \omega + (1 - \frac{1}{2} \frac{\|\psi\|}{\tan(\frac{1}{2}\|\psi\|)})[\psi]^2 \cdot \omega / \|\psi\|^2$ ,  $\dot{\omega} = J^{-1}(\rho(f_2 - f_4)\mathbf{e}_x) + \rho(f_3 -$   
 $f_1)\mathbf{e}_y + k_m(f_1 - f_2 + f_3 - f_4)\mathbf{e}_z - [\omega] \cdot J \cdot \omega$ ,  $g = 9.8ms^{-2}$  and  $\mathbf{e}_i$ ,  $i = x, y, z$  stand  
 for standard basis vectors in  $\mathbb{R}^3$ ,  $k_v, m, J, \rho$  and  $k_m$  are robot specific constants.

### 2.2. Empirical Model

155 Other than the exact model, a 6-DOF motion model was proposed for gov-  
 erning quadrotor in a distributed setup [69]. Later, it was reduced to 4-DOF

160 motion model [5]. Furthermore, in [70], a 4-DOF motion was used for controlling several quadrotors in a distributed setup in which NMPC and Model Horizon Estimation (MHE) are incorporated for relative tracking where the relative motion model was defined as:

$$\dot{\mathbf{x}} = \mathbf{f}_c(\mathbf{x}, \mathbf{u}, \psi_z) = \begin{bmatrix} \dot{\mathbf{p}}_x \\ \dot{\mathbf{p}}_y \\ \dot{\mathbf{p}}_z \\ \dot{\psi}_z \end{bmatrix} = \begin{bmatrix} \mathbf{v}_x \cos(\psi_z) - \mathbf{v}_y \sin(\psi_z) - \bar{\mathbf{v}}_x + \mathbf{p}_y \dot{\bar{\psi}}_z \\ \mathbf{v}_x \sin(\psi_z) + \mathbf{v}_y \cos(\psi_z) - \bar{\mathbf{v}}_y - \mathbf{p}_x \dot{\bar{\psi}}_z \\ \mathbf{v}_z - \bar{\mathbf{v}}_z \\ \dot{\psi}_z - \dot{\bar{\psi}}_z \end{bmatrix}, \quad (1)$$

where the function  $\mathbf{f}_c(\cdot) : \mathbb{R}^{n_u} \times \mathbb{R}^{n_x} \times \mathbb{R}^{n_{ru}} \rightarrow \mathbb{R}^{n_x}$  and  $n_x = n_u = n_{ru} = 4$ . The current control input is given by  $\mathbf{u} = [\mathbf{v}_x, \mathbf{v}_y, \mathbf{v}_z, \dot{\psi}_z]$ , whereas relative control input  $\mathbf{u}_{ru}$  is denoted by  $[\bar{\mathbf{v}}_x, \bar{\mathbf{v}}_y, \bar{\mathbf{v}}_z, \dot{\bar{\psi}}_z]$ .  $\mathbf{x} = [\mathbf{p}_x, \mathbf{p}_y, \mathbf{p}_z, \psi_z]$  is the state of the motion model, where  $\mathbf{p}_i, i \in \{x, y, z\}$  is the position of the MAV in the world frame.  $\psi_z$  and  $\bar{\psi}_z$  denote the yaw angle or heading angle around the z axis and relative yaw angle, respectively. Derivative of  $\psi_z$  and  $\bar{\psi}_z$  are denoted by  $\dot{\psi}_z$  and  $\dot{\bar{\psi}}_z$ , respectively.  $\mathbf{v}_i, i \in \{x, y, z\}$  denote the velocities on each direction, whereas  $\dot{\mathbf{p}}_i, i \in \{x, y, z\}$  gives the derivatives of  $\mathbf{p}_i$ . Since discrete space was chosen for controlling the system, Euler discrete model (1) was formulated as follows:

$$\mathbf{x}^+ = \mathbf{f}_d(\mathbf{x}, \mathbf{u}, \psi_z) = \begin{bmatrix} p_x \\ p_y \\ p_z \\ \psi_z \end{bmatrix} + \delta \begin{bmatrix} v_x \cos(\psi_z) - v_y \sin(\psi_z) - \bar{v}_x + y \dot{\bar{\psi}}_z \\ v_x \sin(\psi_z) + v_y \cos(\psi_z) - \bar{v}_y - x \dot{\bar{\psi}}_z \\ v_z - \bar{v}_z \\ \dot{\psi}_z - \dot{\bar{\psi}}_z \end{bmatrix}, \quad (2)$$

where  $\delta$  is the sampling period and  $\mathbf{f}_d(\cdot) : \mathbb{R}^{n_x} \times \mathbb{R}^{n_u} \times \mathbb{R}^{n_{ru}} \rightarrow \mathbb{R}^{n_x}$ .  $\mathbf{f}_c$  and  $\mathbf{f}_d$  denote continuous and discrete dynamics, respectively.  $\mathbf{x}^+$  depicts the next state given the current state  $\mathbf{x}$ . Subsequently, the motion model was simplified to 4-DOF for trajectory tracking for a quadrotor [71, eq.(1)]. In this trajectory-tracking approach, planning followed by the high-level controlling paradigm was applied. Such an approach was introduced because a simplified motion model is a reasonable choice for achieving real-time performance. Quadrotor state was defined as  $\mathbf{x} = [\mathbf{p}_x, \mathbf{p}_y, \mathbf{p}_z, \psi_z]^T \in \mathbb{R}^{n_x}$ , whereas input to the system was given

by  $\mathbf{u} = [\mathbf{v}_x, \mathbf{v}_y, \mathbf{v}_z, \dot{\psi}_z]^T \in \mathbb{R}^{n_u}$ . The simplified motion model was given by

$$\dot{\mathbf{x}} = \mathbf{f}_c(\mathbf{x}, \mathbf{u}) = \begin{bmatrix} \dot{\mathbf{p}}_x \\ \dot{\mathbf{p}}_y \\ \dot{\mathbf{p}}_z \\ \dot{\psi}_z \end{bmatrix} = \begin{bmatrix} \mathbf{v}_x \cos(\psi_z) - \mathbf{v}_y \sin(\psi_z) \\ \mathbf{v}_x \sin(\psi_z) + \mathbf{v}_y \cos(\psi_z) \\ \mathbf{v}_z \\ \dot{\psi}_z \end{bmatrix}, \quad (3)$$

where  $\mathbf{f}_c(\cdot) : \mathbb{R}^{n_x} \times \mathbb{R}^{n_u} \rightarrow \mathbb{R}^{n_x}$  and  $n_x = n_u = 4$ . The discretization of (3) was given by:

$$\mathbf{x}^+ = \mathbf{f}_d(\mathbf{x}, \mathbf{u}) = \begin{bmatrix} \mathbf{p}_x \\ \mathbf{p}_y \\ \mathbf{p}_z \\ \psi_z \end{bmatrix} + \delta \begin{bmatrix} \mathbf{v}_x \cos(\psi_z) - \mathbf{v}_y \sin(\psi_z) \\ \mathbf{v}_x \sin(\psi_z) + \mathbf{v}_y \cos(\psi_z) \\ \mathbf{v}_z \\ \dot{\psi}_z \end{bmatrix}, \quad (4)$$

where  $\mathbf{f}_d(\cdot) : \mathbb{R}^{n_x} \times \mathbb{R}^{n_u} \rightarrow \mathbb{R}^{n_x}$ .

### 2.3. Differential Flatness

Here differential flatness [72] provides algebraic functions (e.g., polynomials) which analytically map the trajectory and whose higher-order derivatives map to system states and inputs. Since the Nth order polynomial can be differentiated up to N-1 times, the differential flatness property ensures the feasibility of the trajectory and generates appropriate control commands. More precisely, let

$$\dot{\mathbf{x}} = \mathbf{f}_c(\mathbf{x}, \mathbf{u}) \quad \mathbf{x} \in \mathbb{R}^{n_x}, \mathbf{u} \in \mathbb{R}^{n_u}. \quad (5)$$

be a nonlinear system. According to [73], if the system is differentially flat, there always exists a flat output, namely  $\mathbf{z} \in \mathbb{R}^{n_z}$ , where the dimension of the output is given by  $n_z$ . In such a system, states and control inputs can also be formulated from the system flat outputs whose derivatives are mapped through functions, namely  $\varrho$  and  $\tau$ . Let  $\mathbf{z} = \mathfrak{F}(\mathbf{x}, \mathbf{u}, \dot{\mathbf{u}}, \dots, \mathbf{u}^{(g)})$  be the flat output, holding  $\mathbf{x} = \varrho(\mathbf{z}, \dot{\mathbf{z}}, \dots, \mathbf{z}^{(r)})$  and  $\mathbf{u} = \tau(\mathbf{z}, \dot{\mathbf{z}}, \dots, \mathbf{z}^{(r)})$ , where apices  $^{(i)}$  stipulates the  $i$ th derivative. Along with that, the explicit trajectory generation process can benefit when it uses differentially flat systems, for example,  $\varrho$  and  $\tau$  can be a  $d$ th order polynomial  $p(t)$ . Then,  $\mathbf{x}^\top(t) = [p^\top(t) \dot{p}^\top(t) \ddot{p}^\top(t)]$  be

the state of the system at time  $t$  in which  $\dot{p}^T$  and  $\ddot{p}^T$  indicate the velocity and acceleration of the system, respectively. Control inputs can be determined by jerk [74], namely  $\ddot{p}^T(t)$  where  $p(t) = \lambda_d t^d + \dots + \lambda_1 t + \lambda_0$ ,  $t \in [0, dt]$ , where  $\lambda_i, i = 0, \dots, d$  are the polynomial coefficients. There are various ways to construct these kinds of polynomials, including Minimum-snap, B-spline, etc.

### 3. Initial Waypoints Identification

Generally speaking, robots have a limited sensing range. So, planning a trajectory out of such a sensing range would be counterproductive. Hence, local trajectory planning and refinement when a robot moves is the optimal choice. With the help of sensing capabilities within the robots' sensing range, the robot's surrounded environment can be constructed as the intersection of three separate disjoint sets: free-known ( $C_{free}$ ), occupied ( $C_{obs}$ ) and unknown ( $C_{unknown}$ ). Once  $C_{free} \cup C_{unknown}$  is identified, a set of intermediate waypoints is needed to navigate the robot along the trajectory from the start position to the desired position. There are various techniques for finding a set of intermediate waypoints: sampling-based techniques (e.g., RRT\*, Probabilistic Road Map (PRM)), path-searching techniques (e.g., A\*, D\*, JPS) and so forth. Moreover, kinodynamic properties are incorporated into preceding intermediate waypoints finding techniques to ensure the dynamic feasibility of the robot. One of the first kinodynamic-based path planning approaches was proposed in [75] in which a variant of the A\* method alongside with kinodynamic properties was applied to ensure the dynamic feasibility. Subsequently, several different methods were proposed for enhancing path planning, ensuring the dynamic feasibility by kinodynamic properties, including motion primitive-based approaches.

Motion primitive-based approaches ([56, 76, 77]) can be utilized for finding intermediate waypoints and for trajectory generation. Gordon et al. [78] proposed a set of motion primitives for connecting edges of the graph that was constructed from A\*. In this method, motion primitives were used to defining state vector  $\mathbf{x}(t)$  and control input  $\mathbf{u}(t)$  as a Linear Time Invariant (LTI) system

as follows:

$$\begin{aligned}\mathbf{x}_i(t) &= [p_i(t)^\top, \dot{p}_i(t)^\top, \dots, p_i^{(k_r-1)}(t)^\top]^\top \in \mathbf{x}_i(t) \subset \mathbb{R}^{3 \times k_r}, \\ p_i(t) &= [p_x(t), p_y(t), p_z(t)]^\top, \mathbf{u}_i(t) = p^{(k_r)}(t),\end{aligned}\tag{6}$$

where  $\mathbf{p}_\mu(t) = \sum_{j=0}^d \lambda_j t^j$ ,  $\mu \in \{x, y, z\}$ , which is formulated similar to (16), while  $k_r$  and  $d$  are the order of the derivative and the order of the polynomial, respectively.

$$\begin{aligned}\dot{\mathbf{x}}_i(t) &= A\mathbf{x}_i(t) + B\mathbf{u}_i(t), \\ A &= \begin{bmatrix} 0 & I_3 & 0 & \cdots & 0 \\ 0 & 0 & I_3 & \cdots & 0 \\ \vdots & \vdots & \vdots & \ddots & \vdots \\ 0 & \dots & \dots & 0 & I_3 \\ 0 & \dots & \dots & 0 & 0 \end{bmatrix}, \quad B = \begin{bmatrix} 0 \\ 0 \\ \vdots \\ 0 \\ I_3 \end{bmatrix}.\end{aligned}\tag{7}$$

Hence, given control policy  $\mathbf{u}_i(t)$  and initial state  $\mathbf{x}(0)$ , a sequence of succeeding states for a given time duration is determined by

$$\mathbf{x}_i(t) = e^{At}\mathbf{x}(0) + \int_0^t e^{A(t-\gamma)} B\mathbf{u}(\gamma) d\gamma,\tag{8}$$

where  $\gamma$  is the time duration that control policy is applied. In [78], to define the actual and heuristic cost of  $A^*$ , the researchers used motion primitives, which are defined (as shown) in (8), and calculated initial waypoints set.

Another interesting approach to finding a set of initial intermediate waypoints is by using fast marching methods. In general, fast marching methods [79] are applied to track the propagation of a convoluted interface such as wavefront, especially in image processing. Let  $\varphi$  be a close curve in a plane  $\in \mathbb{R}^3$  that propagates orthogonally to the plane with a speed  $v(\mathbf{p})$ , assume  $v > 0$ . Given  $\nabla T$  time period, propagation of the plane can be described by  $|\nabla T(x)| = \frac{1}{v(\mathbf{p})}$  based on Eikonal partial differential equation [80] where  $\mathbf{p}$  is the position in  $\mathbb{R}^3$  and the arrival time is formulated by  $T(x)$ . Fast marching concept was applied for path searching in [14] by proposing a method for calculating velocity map. In this method, the arrival time was determined by assessing the desired velocity at the considered position. Hence, arrival time was calculated by backtracking

from the goal pose to the start pose along the minimum cost path, which can be estimated from the gradient descendant. Though gradient descendant may trap in a local minimum, when smart marching is applied, gradient descendant does not trap in local minimum due to fast marching nature; this property was proved in [81]. To define the velocity map, ESDF was utilized to get the closest obstacle poses from the given pose. A quadrotor should move faster when there are no close-in obstacles and should be slower when it is moving through a cluttered environment. Such a behaviour was mimicked by incorporating a hyperbolic tangential function, i.e.,  $\tanh$ . With such an assumption, the corresponding velocity was calculated based on (9)

$$v(l) = \begin{cases} v_{max}(\tanh(l - e) + 1)/2, & 0 \leq l \\ 0, & l < 0 \end{cases}, \quad (9)$$

where  $v_{max}$  is the maximum velocity a quadrotor can fly,  $l$  is the distance to the  
 200 closest obstacle from the considered pose  $\mathbf{p}$  and  $e$  is Euler's constant.

#### 4. Initial Trajectory Generation

Let us consider a non-linear system in the form of  $\dot{\mathbf{x}}(t) = \mathbf{f}_c(\mathbf{x}(t), \mathbf{u}(t))$  with initial state  $\mathbf{x}(t_0) = \mathbf{x}_0$ , where state vector and control inputs are denoted by  $\mathbf{x} \in \mathbf{R}^{n_x}$  and  $\mathbf{u} \in \mathbf{R}^{n_u}$ , respectively. When generating an initial trajectory ( $\Gamma$ ), ensuring dynamic feasibility is a must. In other words,  $\mathbf{x}$  and  $\mathbf{u}$  satisfy the following constraints:

$$\mathbf{x} \in X \subseteq \mathbf{R}^{n_x}, \quad \mathbf{u} \in U \subseteq \mathbf{R}^{n_u} \quad (10)$$

In addition to these constraints, safety constraints should also be imposed after reasoning the environment, to guarantee safety. The environment or configuration space  $C$  can be decomposed into  $C_{obs}$  and  $C_{free}$ . Hence, a set of con-  
 205 straints should be introduced for the quadrotor to always be within free space  $\mathbf{x} \in C_{free} = C / C_{obs}$ . Hence, the initial trajectory generation process has to consider both said types of constraints simultaneously so that the quadrotor would have a smooth flying experience.

#### 4.1. Define Trajectory

210 Let  $\Gamma \leftarrow C \subset \mathbb{R}^d$  be an initial trajectory, which is parameterized as a function of time where  $d$  denotes the  $C$ 's dimension. Since  $\Gamma$  is a function, the objective of the trajectory generator is to determine the precise objective, which will eventually provide the optimal trajectory in a timely manner satisfying constraints and hypotheses that are imposed. Hence, optimal trajectory, namely  
 215  $\Gamma^*$ , can be posed as a discrete or continuous OCP [82]:

$$\begin{aligned}
 \Gamma^* &= \min_{\mathbf{u}(\cdot)} J(\mathbf{x}(0), \mathbf{u}(\cdot)) \\
 \text{s.t. } &\mathbf{x}(0) = \mathbf{x}_0, \mathbf{x}(t_n) = \mathbf{x}_n \\
 &\dot{\mathbf{x}}(t) = \mathbf{f}_c(\mathbf{x}(t), \mathbf{u}(t)) \\
 &\mathbf{x}(t) \in C_{free}, \mathbf{u}(t) \in U, t \in [t_0, t_n],
 \end{aligned} \tag{11}$$

where  $t_0$  and  $t_n$  denote the start and terminal time, respectively. Yet another challenging problem is to formulate the objective function, namely  $J$ . In the following subsections, we discuss several approaches to address this problem.

#### 4.2. Minimum-snap based Trajectory Generation

Minimum-snap trajectory generation [3] uses the differential flatness property (section 2.3) to automate the trajectory generation process. Let quadrotor trajectory be  $\Gamma_T(t) = [r_T(t), \psi_T(t)]^T$  for flat output  $[x, y, z, \psi_z]^T$  where  $r = [x, y, z]$  is the center position of the MAV with respect to world coordinate system and  $\psi_z$  is the yaw angle of the MAV. The continuous trajectory can be expressed as follows:

$$\Gamma(t) : [t_0, t_n] \leftarrow \mathbb{R}^d, \tag{12}$$

220 where  $d$  is the dimension of the space, e.g., 3. As we defined in section 2.3, system states and inputs can be determined in terms of  $\Gamma$  and its derivatives.  $\Gamma, \dot{\Gamma}$  and  $\ddot{\Gamma}$  will correspond to position, velocity and acceleration, respectively. Flat output and its derivatives estimation in Minimum-snap refer to the original work [3, eqs. (1-35)].

In Minimum-snap trajectory parameterization, the total time duration of the trajectory is divided into a set of sub-intervals, i.e., keyframes. Each keyframe consists of a desired position and a yaw angle. A safe corridor is constructed between consecutive keyframes as a set of piecewise polynomial functions to estimate smooth transitions through the keyframes. Let  $m_d$  and  $d$  be the number of keyframes and the order of the piecewise polynomial functions, respectively. Hence,  $\Gamma_T(t)$  can be formulated as

$$\Gamma_T(t) = \begin{cases} \sum_{i=0}^d \Gamma_{i,1}(t-t_0)^i & t_0 \leq t < t_1 \\ \sum_{i=0}^d \Gamma_{i,2}(t-t_1)^i & t_1 \leq t < t_2 \\ \vdots & \\ \sum_{i=0}^d \Gamma_{i,m_d}(t-t_{m_d-1})^i & t_{m_d-1} \leq t < t_{m_d} \end{cases}. \quad (13)$$

To generate an optimal trajectory, the following objective is utilized:

$$\begin{aligned} J(r_T, \psi_T) &= \int_{t_0}^{t_{m_d}} \xi_r \left\| \frac{d^{k_r} r_T}{dt^{k_r}} \right\|^2 dt + \xi_\psi \frac{d^{k_\psi} \psi_T^2}{dt^{k_\psi}} dt \\ \min_w \quad & J(r_T, \psi_T) \\ \text{s.t.} \quad & \Gamma_T(t_i) = \Gamma_i \quad i = 1, \dots, m_d \\ & \frac{d^p x_T}{dt^p} \Big|_{t=t_j} \leq 0 \quad j = 0, m_d; p = 1, \dots, k_r \\ & \frac{d^p y_T}{dt^p} \Big|_{t=t_j} \leq 0 \quad j = 0, m_d; p = 1, \dots, k_r \\ & \frac{d^p z_T}{dt^p} \Big|_{t=t_j} \leq 0 \quad j = 0, m_d; p = 1, \dots, k_r \\ & \frac{d^p \psi_T}{dt^p} \Big|_{t=t_j} \leq 0 \quad j = 0, m_d; p = 1, \dots, k_\psi, \end{aligned} \quad (14)$$

where  $\xi_r$  and  $\xi_\psi$  are regulation parameters,  $k_r$  and  $k_\psi$  are the order of derivation at each keyframe and  $\Gamma_T(t_i) = [x_i, y_i, z_i, \psi_{z_i}]^T$ ,  $i = 0, \dots, T$ . Time intervals,  $t_1, t_2, \dots, t_{m_d}$  can be kept constant or varying when deriving the Minimum-snap trajectory generation. In most cases, having varying time intervals between keyframes is necessary. Mellinger et al. [3] proposed a gradient descent-based approach for finding optimal time intervals between keyframes. Further, Chen et al. [13] utilized A\* to find the intermediate waypoints. Based on these estimations, time segments or keyframes are calculated incorporating both velocity



and acceleration limits. In the latter approach, the steps listed below were used to obtain intermediate waypoints. Initially, the environment was constructed as a map using OctoMap. Afterwards, the formed map was split into two subsets: allocated and non-allocated (a set of free spaces). Then, the discrete graph was constructed connecting consecutive free spaces, which were represented as cubes. Afterwards, A\* was applied for finding the optimal path segment within each cube. Similar to (14), the researchers set  $k_r = 3$  and minimized only total jerk (15) to minimize the angular velocity. As an aside, minimizing the angular velocity helps to avoid fast rotation.

$$J = \int_{t_0}^{t_{m_d}} \xi_r \left\| \frac{d^{k_r} \Gamma_T(t)}{dt^{k_r}} \right\|^2 dt. \quad (15)$$

#### 225 4.3. Polynomial Trajectory Generation as QP

In Minimum-snap trajectory generation, total trust force, i.e., attitude acceleration, is proportional to the fourth derivative (snap) of the trajectory [3]. The gracefulness of such behaviour helps to avoid generating excessive control commands. Subsequently, a slight variation of Minimum-snap trajectory generation was proposed in [51], where segment times or keyframes were fixed initially. Once start and goal positions were provided, RRT\* [22] was utilized for finding an obstacle-free path between the start and the goal poses as a sequence of optimal waypoints. Initial segment times ( $m_d$ ), which were estimated using optimal waypoints, were calculated according to the maximum velocities that the quadrotor is allowed to fly due to set technical limits. Let  $p_i(t)$  be the  $d$ th order polynomial in the  $i$ th segment that describes as follows:

$$p_i(t) = \lambda_0 t^0 + \lambda_1 t^1 + \lambda_2 t^2 + \lambda_3 t^3 + \dots + \lambda_d t^d. \quad (16)$$

Each  $p_i(t)$  provides a flat output for a given time index  $t$ .  $\lambda_j, j = 0, \dots, d$  denotes the polynomial coefficients. The objective or cost function  $J(\Gamma_i)$  can be fully determined by penalizing the derivatives of squares [51]:

$$J(\Gamma_i) = \int_{t_i}^{t_{i+1}} \xi_0 p_i(t)^2 + \xi_1 \dot{p}_i(t)^2 + \xi_2 \ddot{p}_i(t)^2 + \dots + \xi_{k_r} p^{(k_r)}(t)^2 = P_i^T Q(T_i) P_i, \quad (17)$$

where  $P_i$  is a vector whose elements contain polynomial coefficients:  $\xi_0, \xi_1, \dots, \xi_{k_r^i}$ ,  $k_r^i$  is the highest order of derivative and  $Q(T_i)$  is Hessian matrix, which contains the  $i$ th segment squares of derivatives. Since there are  $m_d$  number of segments, total cost  $J(\Gamma)$  can be expressed by

$$J(\Gamma) = \begin{bmatrix} P_1 \\ \vdots \\ P_{m_d} \end{bmatrix}^T \begin{bmatrix} Q(T_1) & & \\ & \ddots & \\ & & Q(T_{m_d}) \end{bmatrix} \begin{bmatrix} P_1 \\ \vdots \\ P_{m_d} \end{bmatrix}. \quad (18)$$

For a smooth flight experience, ensuring the continuity of derivatives between segments is necessary. Hence, imposing constraints between segments, e.g., velocity, acceleration, jerk and snap is needed, which can be formulated as follows:

$$C_i p_i = \mathbf{d}_i, \quad C_i = \begin{bmatrix} \xi_0 \\ \vdots \\ \xi_{k_r} \end{bmatrix}_i, \quad \mathbf{d}_i = \begin{bmatrix} d_0 \\ \vdots \\ d_{k_r} \end{bmatrix}_i, \quad (19)$$

where  $C_i$  contains a mapping matrix whose entries contain the start and end coefficients of  $i$ th segment, whereas  $d_i$  contains derivative values, i.e., start and end of  $i$ th segment. Taking all constraints of  $m_n$  segments,

$$C \begin{bmatrix} p_1 \\ \vdots \\ p_{m_d} \end{bmatrix} = \begin{bmatrix} \mathbf{d}_1 \\ \vdots \\ \mathbf{d}_{m_d} \end{bmatrix}. \quad (20)$$

Now this can be solved as a constrained QP problem.

#### 4.4. Unconstrained Polynomial Trajectory Generation

The techniques that are used for unconstrained trajectory optimization are faster than constraints optimization. In [51], the researchers extended Minimum-snap trajectory generation as an unconstrained QP. According to their findings, Minimum-snap works well for small segments size. For higher-order polynomials with varying segment sizes, Minimum-snap becomes ill-conditioned. Thus, an unconstrained QP was proposed. After substituting (19) and (20) into (18),

$J(\Gamma)$  can be reformulated as

$$\begin{aligned}
J(\Gamma) &= \underbrace{\begin{bmatrix} \mathbf{d}_1 \\ \vdots \\ \mathbf{d}_{m_d} \end{bmatrix}}_{\mathbf{d}} \underbrace{\begin{bmatrix} C(T_1) & & \\ & \ddots & \\ & & C(T_{m_d}) \end{bmatrix}}_{C^{-T}} \underbrace{\begin{bmatrix} Q(T_1) & & \\ & \ddots & \\ & & Q(T_{m_d}) \end{bmatrix}}_Q \\
&= \begin{bmatrix} \mathbf{d}_f \\ \mathbf{d}_p \end{bmatrix}^T \underbrace{SC^{-T}QC^{-1}S^T}_R \begin{bmatrix} \mathbf{d}_f \\ \mathbf{d}_p \end{bmatrix} = \begin{bmatrix} \mathbf{d}_f \\ \mathbf{d}_p \end{bmatrix}^T \begin{bmatrix} R_{ff} & R_{fp} \\ R_{pf} & R_{pp} \end{bmatrix} \begin{bmatrix} \mathbf{d}_f \\ \mathbf{d}_p \end{bmatrix}, \quad (21)
\end{aligned}$$

where  $\mathbf{d}$  contains fixed derivatives ( $\mathbf{d}_f$ ) and free derivatives ( $\mathbf{d}_p$ ),  $S$  is a permutation matrix (ones and zeros), which is used to correct the order. Then,  $\frac{dJ(\Gamma)}{d\mathbf{d}_p} = 0$  yields the optimal value for  $\mathbf{d}_p$ :

$$\mathbf{d}_p^* = -R_{pp}^{-1}R_{fp}^T \mathbf{d}_f. \quad (22)$$

Once  $\mathbf{d}_p$  is determined, a polynomial that corresponds to each segment can be recovered.

#### 230 4.5. Unconstrained Polynomial Trajectory Generation with Collision Avoidance

Oleynikova et al. [53] extended what Richter [51] proposed for adding support for collision avoidance capabilities. They added additional term for calculating the collision cost,

$$\begin{aligned}
J(\Gamma) &= \xi_{obs} J_{obs}(\Gamma) + \xi_{smooth} J_{smooth}(\Gamma), \quad (23) \\
J_{smooth} &= \mathbf{d}_f^T R_{ff} + \mathbf{d}_f^T R_{fp} \mathbf{d}_p + \mathbf{d}_p R_{pf} \mathbf{d}_f + \mathbf{d}_p^T R_{pp} \mathbf{d}_p,
\end{aligned}$$

where  $J_{smooth}$  exactly equals (21). To estimate  $J_{obs}(\Gamma)$ , it is required to initially calculate position  $\mathbf{p}_i(t)$  (16) and velocity  $\mathbf{v}_i(t)$  for each axis at time  $t$  after

selecting the corresponding segment ( $i, i = 1, \dots, m_d$ )

$$\begin{aligned} \mathbf{p}_i(t) &= Tp_i, \quad p_i = [\lambda_0, \lambda_1, \dots, \lambda_d]_i^T, \quad T = [t^0, t^1, t^2, \dots, t^d], \\ \mathbf{v}_i(t) &= \dot{\mathbf{p}}_i(t) = TVp_i, \end{aligned} \quad (24)$$

$$\mathbf{p}_i(t) = [\mathbf{p}_x(t) \ \mathbf{p}_y(t) \ \mathbf{p}_z(t)]_i, \quad \mathbf{v}_i(t) = [\mathbf{v}_x(t) \ \mathbf{v}_y(t) \ \mathbf{v}_z(t)]_i.$$

Knowing (the values of)  $\mathbf{p}_i(t)$  and  $\mathbf{v}_i(t)$ ,  $J_{obs}(\Gamma_i)$  can be fully determined by

$$\begin{aligned} J_{obs}(\Gamma_i) &= \int_S c(\mathbf{p}_i(t)) ds = \int_{t=0}^{t^d} c(\mathbf{p}_i(t)) \|\mathbf{v}_i(t)\| dt = \sum_{t=0}^{t^d} c(\mathbf{p}_i(t)) \|\mathbf{v}_i(t)\| \Delta t \\ \frac{\partial J_{obs}(\Gamma_i)}{\partial d\mathbf{p}_i(t)} &= \sum_{t=0}^{t^d} \|\mathbf{v}_i(t)\| \nabla_i c(T(C^{-1}S)_{pp}) \Delta t + c(\mathbf{p}_i(t)) \frac{\mathbf{v}_i(t)}{\|\mathbf{v}_i(t)\|} TV(C^{-1}S)_{pp} \Delta t, \end{aligned} \quad (25)$$

where  $(C^{-1}S)_{pp}$  is the right-side matrix which corresponds to  $\mathbf{d}_p$ . For representing the collision cost  $c(\mathbf{p}_i(t))$ , a line integral of a potential function, i.e., (44), was used. As total cost is given (21),  $J_{obs}(\Gamma)$  can be calculated for all the segments provided that  $\mathbf{d}_p^*$  can be estimated. In a cluttered environment, optimization problem is most likely to be non-linear as well as non-convex. Thus, Broyden—Fletcher—Goldfarb—Shanno (BFGS) [83] was used to solve the optimization problem. Yet the solver failed to obtain the global minimum most of the time. Hence, several random restarts were needed to find the optimal solution. A thorough discussion of how random restarts were invoked into the optimization problem was detailed in [59].

#### 4.6. Covariant Gradients for Trajectory Generation

The significance of covariant gradients technique is that both  $J_{obs}(\Gamma)$  and  $J_{smooth}(\Gamma)$  depend solely on physical characteristic of the desired trajectory. In other words, the trajectory generation is invariant to its parameterization. If gradient descent is applied, it depends on the way trajectory is parameterized. The covariant gradients technique removes this dependency. Hence, covariant gradient technique depends solely on physical representation or dynamic quantities of the trajectory with respect to an operator,  $\Theta$ .

$$\|\Gamma\|_{\Theta}^2 = \int \sum_{n=1}^k \xi(\Gamma(t)^{(n)})^2 dt, \quad (26)$$

where  $\xi$  is a constant and apices  $^{(n)}$  determine the  $n$ th order derivative. The correlation of derivatives between two trajectories:  $\Gamma_1$  and  $\Gamma_2$ , is defined by assuming inner product as given (27).

$$\langle \Gamma_1, \Gamma_2 \rangle = \int \sum_{n=1}^k \xi \Gamma_1(t)^{(n)} \Gamma_2(t)^{(n)} dt. \quad (27)$$

245 The primary objective of  $\Theta$  is to distinguish the norm (26) and the inner product (27) from the L2 norm [63].

#### 4.7. B-spline based Trajectory Generation

$d^{th}$  order B-spline can be defined for a given knot sequence  $p_k = \{t_0, t_1, \dots, t_{n_k}\}$  and control points  $p_c = \{\mathbf{p}_0, \mathbf{p}_1, \dots, \mathbf{p}_{n_p}\}$ , where  $t_* \in \mathbb{R}$ ,  $\mathbf{p}_* \in \mathbb{R}^d$  and  $n_k = n_p + d + 1$ . If  $d$  is set to 3, each  $\mathbf{p}_i$  represents position in  $\mathbb{R}^3$ , where  $i = 0, \dots, n_p$ . For a given time index  $t$ , the corresponding position  $\mathbf{p}(t)$  can be fully determined by using De-Boor-Cox formula [84].

$$\mathbf{p}(t) = DeBoorCox(t, p_c). \quad (28)$$

Estimation is not limited to the position; velocity, acceleration or any high order derivative of  $p_c$  can be estimated using  $DeBoorCox(t, p_c^{(*)})$  as given in 250 Algorithm. 1, where  $^{(*)}$  depicts the order of the derivative of  $p_c$  such that  $(*) < d$ .

Later, the B-spline matrix representation was proposed by Qin [85]. B-spline can be formulated as uniform or non-uniform. J. Hu et al. [86] detailed the uniform B-spline matrix representation. In uniform B-spline, knot span is the same for any considered consecutive time interval, i.e.,  $\Delta t = t_{i+1} - t_i$ ,  $i \in [0, n_k)$ . Any position of the trajectory can be parameterized by considering only  $d+1$  consecutive control points:  $[\mathbf{p}_i, \mathbf{p}_{i+1}, \dots, \mathbf{p}_{i+d}]$ . Hence, corresponding normalized time  $q(t)$  can be calculated as follows:

$$q(t) = \frac{t - t_i}{t_{i+1} - t_i} = \frac{t - t_i}{\Delta t}, \quad t \in [t_i, t_{i+1}]. \quad (29)$$

In the matrix representation,  $c(q(t))$ , which is given in (28), can be determined

---

**Algorithm 1** The B-spline trajectory ( $p$ ) and its derivative estimation for a given time index  $t$ , where  $p$  equals  $p_c^{(*)}$

---

```

1: procedure DEBOORCOX( $t, p$ )
2:    $t = \begin{cases} p_k[d], & \text{if } t < p_k[d] \\ p_k[n_k], & \text{if } t > p_k[n_k] \\ t, & \text{otherwise} \end{cases}$ 
3:    $k = d$ 
4:   while true do
5:     if  $p_k[k + 1] \geq t$  then
6:       break
7:      $k++$ 
8:      $\mathbf{p}_e[d]$ 
9:     for  $i \leftarrow 0$  to  $d$  do
10:       $\mathbf{p}_e[i] \leftarrow p[k - d + i]$ 
11:     for  $r \leftarrow 1$  to  $d$  do
12:       for  $i \leftarrow d$  to  $r$  do
13:          $\beta \leftarrow \frac{t - p_k[i+k-d]}{p_k[i+1+k-r] - p_k[i+k-d]}$ 
14:          $\mathbf{p}_e[i] \leftarrow (1 - \beta) \times \mathbf{p}_e[i - 1] + \beta \times \mathbf{p}_e[i]$ 
15:     return  $\mathbf{p}_e[d]$ 

```

---

by:

$$c(q(t)) = \mathbf{q}(t)M_d p_i, \quad \mathbf{q}(t) = [1, q(t), q^2(t), \dots, q^d(t)]^T, \quad p_i = [\mathbf{p}_i, \mathbf{p}_{i+1}, \dots, \mathbf{p}_{i+d}]^T, \\ M_d \in \mathbb{R}^{d+1 \times d+1}, \quad M_{r,c} = \frac{1}{d!} \binom{d}{d-r} \sum_{s=c}^d (-1)^{s-c} \times \binom{d}{s-c} (d-s)^{d+1-r-s}. \quad (30)$$

Since each control point  $\mathbf{p}_i$  belongs to  $d + 1$  of successive spans, B-spline can be controlled locally. Due to such controllability, b-spline is suitable for local trajectory planning [26]. Moreover, the derivatives of a given B-spline are also B-spline [11]. Hence, B-spline's derivatives (e.g., velocity, acceleration, jerk) can be calculated considering corresponding span  $[t_i, t_i + 1)$  for a given  $d+1$  consecutive control points  $p_i = [\mathbf{p}_i, \mathbf{p}_{i+1}, \dots, \mathbf{p}_{i+d}]^T \in \mathbb{R}^{d \times 3}$  and corresponding knot vector.

$$\frac{dc(q(t))}{du} = \frac{1}{(\Delta t)} b_1 M_d \mathbf{v}_i^T, \quad b_1 = [0, 1, u, \dots, u^{d-1}] \in \mathbb{R}^{d+1}, \\ \frac{d^2 c(q(t))}{d^2 u} = \frac{1}{(\Delta t^2)} b_2 M_d \mathbf{v}_i^T, \quad b_2 = [0, 0, 1, u, \dots, u^{d-2}] \in \mathbb{R}^{d+1}. \quad (31)$$

The explicit form of estimation of velocity and acceleration of a given time index is calculated as follows:

$$\frac{dc(q(t))}{du} = d \cdot \frac{p_c(i+1) - p_c(i)}{p_k(i+d+1) - p_k(i+1)}, \\ \frac{d^2 c(q(t))}{d^2 u} = (d^2 - d) \cdot \left( \frac{p_c(i+2) - p_c(i+1)}{p_k(i+d+2) - p_k(i+2)} - \frac{p_c(i+1) - p_c(i)}{p_k(i+d+1) - p_k(i+1)} \right). \quad (32)$$

In most of the situations, initial control points are generated as explained in section 3. Such methods may or may be not smooth enough for initial trajectory generation. There are various ways to generate intermediate waypoints to improve the quality of the trajectory using B-splines. For example, the initial trajectory was constructed using cubic B-Spline in [71]. Such a capability is mainly due to B-spline's properties.

It is particularly continuity and convex-hull properties that make B-spline trajectory generation such a robust technique.

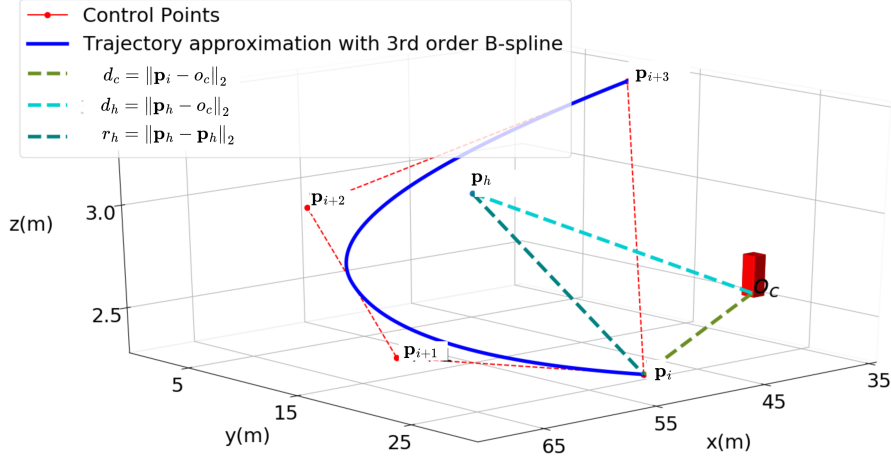


Figure 5: Showing the B-spline convex-hull property. Convex hull, which comprises consecutive control points, e.g.,  $\mathbf{p}_i, \mathbf{p}_{i+1}, \mathbf{p}_{i+2}$  and  $\mathbf{p}_{i+3}$ , always belongs to obstacle-free space if the preceding control points satisfy the inequality (33)

#### 4.7.1. Convex Hull Property

Among the properties of the B-spline, the convex hull property is the most significant property due to its capabilities for checking the dynamical feasibility and the collision. How convex hull property is incorporated for calculating dynamical feasibility is given in (32). As shown in Fig. 5,  $d_h > 0$  and  $d_h > d_c - r_h$  should be held for a considered point in the trajectory to ensure a collision-free trajectory, where  $d_c$  is the distance between a given control point and its closest obstacle position. In  $d$ th order B-spline, a convex hull is formed by connecting any successive  $d + 1$  control points, e.g.,  $\mathbf{p}_i, \mathbf{p}_{i+1}, \mathbf{p}_{i+2}, \dots, \mathbf{p}_{i+d}$  or union of all consecutive control points that lie on the corresponding b-spline curve [78]. Moreover,  $r_h$  can be substituted with  $d_{i,i+1} + d_{i+1,i+2} + d_{i+2,i+3}$  since  $r_h \leq d_{i,i+1} + d_{i+1,i+2} + d_{i+2,i+3}$ ,  $d_h > d_c - (d_{i,i+1} + d_{i+1,i+2} + d_{i+2,i+3})$ , where  $d_{i,i+1} = \|\mathbf{p}_{i+1} - \mathbf{p}_i\|$ ,  $d_{i+1,i+2} = \|\mathbf{p}_{i+2} - \mathbf{p}_{i+1}\|$  and  $d_{i+2,i+3} = \|\mathbf{p}_{i+3} - \mathbf{p}_{i+2}\|$ . As mentioned in [21], the following condition should hold for collision-free tra-



jectory planning:

$$d_{i,i+1} < \frac{d_c}{3}, \quad d_c > 0, \quad i \in \{1, 2, 3\}. \quad (33)$$

260 4.7.2. Continuity

B-spline-based trajectory generation has several advantages over the piecewise-based trajectory generation [51, 53]. The boundary constraints are to be satisfied explicitly to guarantee the continuity of a piece-wise trajectory. In such a trajectory, the smoothness of the trajectory solely depends on the way  
 265 control points are formed. On the other hand, boundary constraints can be neglected since the whole trajectory can be treated as one segment in B-spline-based trajectory generation. Moreover, the B-spline-based trajectory can be controlled locally, as explained in section 4.7.1, without affecting the rest of the trajectory.

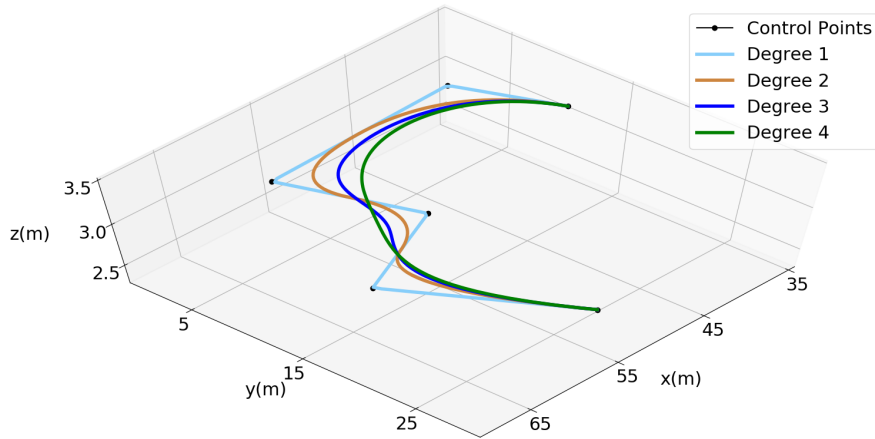


Figure 6: Trajectory generation using uniform B-spline. The smoothness of the curve is dependent on the degree of the B-spline. The trajectory passes precisely through the given control points at the degree equal to 1, as depicted in light blue color. The smoothness of the trajectory increases with the order of the B-spline

Bernstein polynomial is a specific form of B-spline, which is similar to the Bezier curve [87, 88]. Bernstein polynomial can be described as follows:

$$\begin{aligned} \Gamma_j(t) &= \lambda_j^0 p_d^0(t) + \lambda_j^1 p_d^1(t) + \dots + \lambda_j^d p_d^d(t) = \sum_{i=0}^d \lambda_j^i p_d^i(t), \\ p_d^i(t) &= \binom{d}{i} \cdot t^i \cdot (1-t)^{d-i}, \end{aligned} \quad (34)$$

where  $d$  is the degree of the polynomial,  $\lambda_j^0, \lambda_j^1, \dots, \lambda_j^d$  are the control points of  $j$ th polynomial segment and  $t \in [0, 1]$ . Since Bezier is a particular form of B-spline curve, such curves hold convex hull property. Hence, given a sequence of control points, a constrained convex hull can be defined using the control points that are considered. Both the beginning and end of the curve are determined by the first and the last control points, respectively. Further, the derivative of Bezier is also a Bezier curve.

$$\Gamma_\mu(t) = \begin{cases} s_1 \cdot \sum_{i=0}^d \lambda_{1,\mu}^i p_d^i\left(\frac{t-t_0}{s_1}\right) & t_0 \leq t < t_1 \\ s_2 \cdot \sum_{i=0}^d \lambda_{2,\mu}^i p_d^i\left(\frac{t-t_1}{s_2}\right) & t_1 \leq t < t_2 \\ \vdots & \\ s_m \cdot \sum_{i=0}^d \lambda_{m,\mu}^i p_d^i\left(\frac{t-t_{m-1}}{s_m}\right) & t_{m-1} \leq t < t_m \end{cases}, \quad (35)$$

where  $i, j$  refer to  $i^{\text{th}}$  control point in  $j^{\text{th}}$  segment, i.e.,  $\lambda_j^i, s_j$  is a scaling factor of  $j^{\text{th}}$  segment for mapping time duration from  $[0, 1]$  to  $[t_{j-1}, t_j]$  and  $\mu \in \{x, y, z\}$ . Once  $\Gamma_\mu(t)$  is obtained, the objective is to minimize the total cost, which can be determined by taking the integral of square error up to  $k_r$  order as given in (15). Such a problem can be formulated as a QP constraint problem. For instance, Gao and Wu [14] proposed a Bernstein-based trajectory optimization approach in which three types of constraints piecewise trajectory continuity, safety constraints which are based on convex hull property, and dynamical feasibility constraints enforced [14].

In the preceding subsections, several types of trajectory parameterization techniques were considered. We have selected three different types of trajectory parameterization techniques for this comparison: piecewise-polynomials

technique, fitting based on a sequence of points, and the third is uniform B-spline-based technique. The objective of piecewise-polynomials is to find optimal polynomial coefficients [3] or end-derivatives [51] of consecutive segments, whereas the objective of the third technique is to find a set of points satisfying the provided constraints [27]. A comparison of how velocity, acceleration, jerk, and snap are varied for selected techniques in terms of mean, standard deviation (std), min and max for the same a set of control points and knot vector is present below. Considered knot vector and control points are

$$\begin{aligned}
 p_{ctrl} = & [[0.011, -0.0329, 2.017], [1.867, 3.408, 1.6], [7.514, 5.715, 3.735], \\
 & [8.410, 0.911, 1.600], [6.902, -5.531, 4.306], [1.899, -6.680, 3.082], \\
 & [-2.302, -0.611, 5.375]] \\
 p_{knot} = & [0.0, 5.0, 12.0, 18.0, 26.0, 31.0, 40]
 \end{aligned} \tag{36}$$

Each approach has its own set of parameters to fine-tune for obtaining an optimal trajectory. The generated trajectories are shown in Fig. 6 with different configuration setup (with different parameter set). Fig. 7 shows how the derivatives up to the 4th change over time on each direction, i.e.,x,y,z, separately for each technique. When looking at the derivatives of each method, it is clear that smoothness, which is the main point to be considered for motion planning, is higher in both B-spline and Minimum-snap compared to CHOMP. Since uniform B-spline is used in this comparison, smoothness changes of each derivative between B-spline and Minimum-snap can not be compared directly due to time allocation when generating the trajectories. Hence, Minimum-snap trajectory smoothness can be changed, optimizing the time allocation process [51]. On the contrary, such a time allocation process is not necessary for uniform B-spline. Yet control points are interpolated appropriately to generate a continuous and smooth trajectory.

We varied the parameter set of each approach appropriately and estimated mean, std, max, min of velocity, acceleration, jerk, and snap profile; the result is given in Table. 1. The results clearly indicate that the consistency of the trajectory depends on the parameters that are used to parameterize the trajec-

tory. Hence, appropriate parameter set selection for a given task is of utmost  
 300 importance, which can be seen by looking at the statistical properties (mean,  
 std, min, and max) of higher-order derivatives, e.g., velocity, acceleration, jerk,  
 and snap. As described in the previous paragraph, the time allocation process  
 directly affects the parameter selection of Minimum-snap. Further, the optimal  
 polynomial coefficients process depends on time allocation as given in (13). On  
 305 the other hand, Poly-traj [51] generation process has fewer parameters to be  
 optimized since it uses free end-derivatives of each segment. Hence, the latter  
 technique is faster than Minimum-snap.

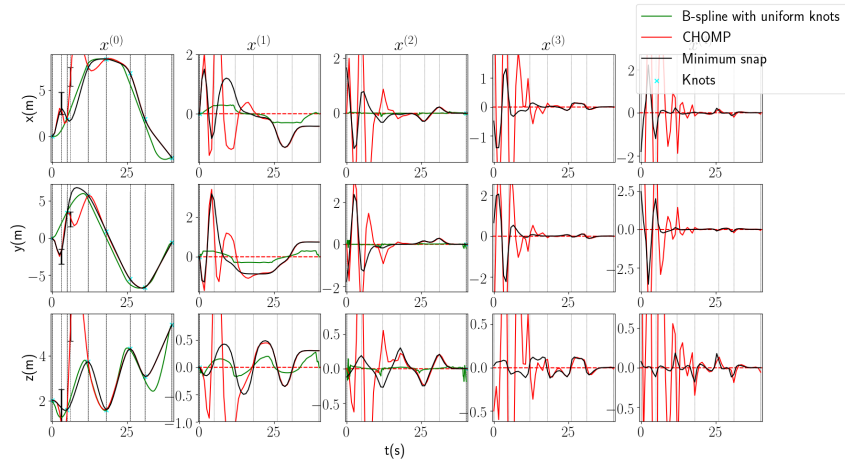


Figure 7: Changes of position, velocity, acceleration, jerk, and snap profiles over time for the provided control points sequence and knot vector (36)

## 5. Free Space Extraction

Obstacle region identification is of utmost essential for optimal trajectory  
 310 planning in real-time. In a cluttered environment, the way the trajectory plan-  
 ning problem formulated is matters for fast reaction. Such trajectory planning  
 approaches can be designed as QP mainly due to less computation power re-

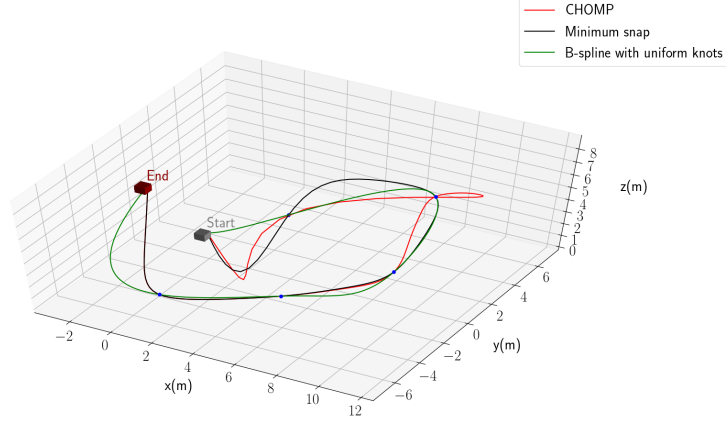


Figure 8: Generated trajectories using three different approaches for a given sequence of control points and knot vector (36)

quired for such tasks. Hence, forming obstacles-free regions in the form of convex has more advantages in terms of reducing the computation power, simplicity and fast convergence. Chen [13] attempted to define free space as a series of cubes  
315 between the start and goal pose. Thenceforth, OctoMap [89] was used for constructing the map surrounding the quadrotor, where regions with no obstacles are considered free spaces. After obtaining the free space information, obstacle constraints are enforced into (15) to generate optimal trajectory.

Let  $C = [c_1^m, c_2^m, \dots]$  be a set of consecutive grids within the OctoMap and corresponding free space regions be  $C_{free} = [c_1^f, c_2^f, \dots]$ . Both  $c_i^m$  and  $c_i^f$  were defined as cubes, each of which is described by

$$c_i^m = \underbrace{[c_{i_{x_0}}^m, c_{i_{y_0}}^m, c_{i_{z_0}}^m]}_{l_m^i}, \underbrace{[c_{i_{x_1}}^m, c_{i_{y_1}}^m, c_{i_{z_1}}^m]}_{u_m^i}, \quad c_i^f = \underbrace{[c_{i_{x_0}}^f, c_{i_{y_0}}^f, c_{i_{z_0}}^f]}_{l_f^i}, \underbrace{[c_{i_{x_1}}^f, c_{i_{y_1}}^f, c_{i_{z_1}}^f]}_{u_f^i}, \quad (37)$$

320 Once  $C_{free}$  was obtained, free space regions can be considered as a set of inequality constraints that can be added into the piece-wise polynomials trajectory generation as  $l_f^i \leq \Gamma_T(t_i) \leq u_f^i$ , where  $i = 1, \dots, m_d - 1$  and  $\Gamma_T$  was defined (13).

Table 1: Velocity, acceleration, jerk, and snap profile for generating an optimal trajectory for a given set of knot vector and control points (Fig. 7) using three different techniques: Minimum-snap [3], Poly-traj [51], and CHOMP [27]

Type	Velocity				Acceleration			
	mean	std	min	max	mean	std	min	max
Poly-traj, d: 8, mc: 2	0.0058	1.0154	-1.4545	3.9179	0.0056	0.9051	-2.835	3.6449
Poly-traj, d: 8, mc: 6	0.0	0.0	0.0	0.0	0.0	0.0	0.0	0.0
Poly-traj, d: 6, mc: 4	0.006	1.0708	-1.7716	3.7864	0.0043	0.9307	-2.7987	3.6032
Poly-traj, d: 8, mc: 4	0.0059	1.0299	-1.4728	3.934	0.0053	0.9131	-2.9157	3.5214
Poly-traj, d: 10, mc: 4	0.0058	1.0057	-1.4428	3.9213	0.0052	0.8918	-2.7541	3.631
Minimum-snap, d: 8, mc: 2	0.1258	1.2154	-1.4345	3.1259	0.0676	0.1259	-2.2874	3.3278
Minimum-snap, d: 8, mc: 6	0.0045	0.0094	-0.07	0.019	0.09	0.0097	-0.0098	0.0014
Minimum-snap, d: 6, mc: 4	0.0689	1.0009	-1.3416	3.2388	0.0012	0.4584	-2.3189	3.2185
Minimum-snap, d: 8, mc: 4	0.0015	1.0412	-1.3215	3.7543	0.0075	0.8763	-2.5487	3.3215
Minimum-snap, d: 10, mc: 4	0.0036	1.0006	-1.3428	3.7832	0.0099	0.4378	-2.4548	3.4893
CHOMP, pd: 3	0.0068	0.6421	-0.9522	1.7255	0.0045	0.3876	-1.131	1.476
CHOMP, pd: 5	0.0065	0.644	-0.9634	1.7161	0.0044	0.3909	-1.1082	1.4418
CHOMP, pd: 7	0.0064	0.6443	-0.966	1.7105	0.0043	0.3916	-1.0951	1.4205
Type	Jerk				Snap			
	mean	std	min	max	mean	std	min	max
Poly-traj, d: 8, mc: 2	0.007	1.2544	-4.8056	3.9318	-0.0151	2.3178	-9.8029	6.9483
Poly-traj, d: 8, mc: 6	0.0	0.0	0.0	0.0	0.0	0.0	0.0	0.0
Poly-traj, d: 6, mc: 4	0.0117	1.568	-5.5746	5.7423	-0.1288	3.5271	-13.4562	10.2578
Poly-traj, d: 8, mc: 4	-0.0021	1.2562	-4.7192	3.7562	0.0131	1.9593	-7.7131	6.0049
Poly-traj, d: 10, mc: 4	0.0074	1.3399	-5.5769	4.409	-0.0504	3.1073	-12.3429	9.9933
Minimum-snap, d: 8, mc: 2	0.0006	1.1125	-4.3413	3.5153	-0.0042	2.1383	-9.0056	6.3418
Minimum-snap, d: 8, mc: 6	0.0005	0.0004	-0.0007	0.0089	0.0005	0.004	-0.0008	0.0009
Minimum-snap, d: 6, mc: 4	0.01	1.3456	-5.2167	5.321	-0.0093	3.214	-12.5124	9.2134
Minimum-snap, d: 8, mc: 4	-0.001	1.1321	-3.7192	3.3217	0.0093	1.2145	-5.6527	4.7854
Minimum-snap, d: 10, mc: 4	0.0009	1.2145	-3.9987	3.9983	-0.0067	2.8731	-10.7653	8.8416
CHOMP, pd: 3	0.0021	0.3643	-1.2594	1.1584	-0.0014	0.4239	-1.8326	1.5425
CHOMP, pd: 5	0.0023	0.3628	-1.2553	1.1639	0.0005	0.4241	-1.8526	1.6243
CHOMP, pd: 7	0.0022	0.3614	-1.2732	1.1769	0.0021	0.4247	-1.7462	1.5906

d: order of the polynomial, mc: maximum continuity or maximum continuity order in between consecutive segments, pd: number of proposed points or point density per defined time duration of the trajectory

In such a trajectory, additional boundary constraints should be introduced if the extrema of  $dth$  order polynomial violates the boundary constraints corresponding to each axis, i.e., x, y and z in each segment [13, eq.10]. Similar to the preceding approach, Gao and Shen [15] proposed a sequence of spheres to

represent free space from the initial position to the final position. To construct the environment, a map was not built; instead, they bypassed map building by constructing a KD-tree [12] based placeholder to store raw point cloud for the LiDAR. Afterwards, a relative map to the current pose of the MAV was  
 330 retrieved using nearest neighbour search; RRG [90] combined with A\* was used to find a flight corridor or intermediate waypoints. Such intermediate waypoints were connected by overlapping spheres.

IRIS [7] is one of the first successful ideas in which obstacle-free spaces are  
 335 extracted using a convex optimization technique. In this proposed approach, initially, it is required to provide a seeking point and an area with a boundary box where an obstacle-free region is to be searched. Seeking point is defined as a unit ball:  $\varepsilon(C, \mathbf{p}_0) = \{\mathbf{p} = C\tilde{\mathbf{p}} + \mathbf{p}_0 \mid \|\tilde{\mathbf{p}}\|_2 \leq 1\}$ , where  $\mathbf{p}_0$  is the center point. The linear constraints, which separate the boundary box into obstacle-free and  
 340 obstacle-rich regions, are defined as a set of hyper-planes:  $P = \{\mathbf{p} \mid A\mathbf{p} \leq b\}$ . Subsequently, finding the optimal representation of  $\varepsilon(C, \mathbf{p}_0)$  and  $P$  with respect to given obstacles,  $\iota_j, j = 1, \dots, N$  is solved as an iterative process (38).

$$\begin{aligned} \min_{C, \mathbf{p}_0, A, \mathbf{b}} \quad & -\log(\det C) \\ \text{s.t.} \quad & A_j^T \mathbf{p}_k \geq \mathbf{b}_j \quad \forall \mathbf{p}_k \in \iota_j, \quad j = 1, \dots, N \\ & \sup_{\|\tilde{\mathbf{p}}\|} A_i^T (C\tilde{\mathbf{p}} + \mathbf{p}_0) \leq \mathbf{b}_i \quad \forall i = 1, \dots, N, \end{aligned} \quad (38)$$

where  $A_i$  and  $\mathbf{b}_i$  correspond to  $i$ th row of  $A$  and  $\mathbf{b}$ . The first constraint, i.e.,  $A_j^T \mathbf{p}_k \geq \mathbf{b}_j$ , is imposed to move the obstacle into one side of the plane,  $A_j^T \mathbf{p} = \mathbf{b}_j$ , whereas the second constraint, i.e.,  $\sup_{\|\tilde{\mathbf{p}}\|} A_i^T (C\tilde{\mathbf{p}} + \mathbf{p}_0) \leq \mathbf{b}_i$ , ensures the ellipsoid lies on the other side of the plane. The researchers proposed to solve the (38) as a two-step process: searching, first, for proper constraints (i.e.,  $A_i$  and  $\mathbf{b}_i$ ) and then the maximum volume that satisfies ellipsoid, ensuring preceding constraints. In other words, they attempted to find hyperplanes that separate obstacle regions and free regions. Conceptually, hyperplane separation is done by finding planes that intersect with obstacle boundaries. Afterwards, the ellipsoid is uniformly expanded until it intersects with obstacle boundaries.

Let  $\alpha$  be the scaling factor which defines the expansion. Let  $\varepsilon_\alpha = \{C\tilde{\mathbf{p}} + \mathbf{p}_0 \mid \|\tilde{\mathbf{p}}\|_2 \leq \alpha\}$  for  $\alpha \geq 1$  be the expanded ellipsoid. Hence, the optimal  $\alpha^*$  can be determined by

$$\begin{aligned} \alpha^* &= \underset{\alpha}{\operatorname{arg\,min}} \\ \text{s.t. } &\varepsilon_\alpha \cap v_j \neq \emptyset \end{aligned} \tag{39}$$

After finding  $\alpha^*$ , it is possible to define the optimal inscribed ellipsoid ( $\varepsilon^*$ ), which is the obstacle-free region [7, sec.3.3].

345 Sikang et al. [17] proposed a new, quite different from the aforesaid IRIS, approach for extracting obstacle-free regions as a convex set SFC. SFC searches a set of overlapping polyhedra from the start pose to the goal pose. To get intermediate obstacle-free positions, the researchers utilized a graph search technique, namely JPS [67]. The main reason for selecting JPS over sampling-based algorithms (e.g., RRT\* and PRM) or search-based techniques such as A\* or Dijkstra 350 is due to the nature of JPS; it uses uniform-cost grid map with uniform voxels. In general, sampling-based techniques are not deterministic though probabilistically complete. Thus, there is no guarantee about the duration of searching time. On the other hand, the computational time for search-based methods is pretty high if the environment is cluttered. However, JPS has a lower searching 355 time compared to A\* [17]. Let  $p_c = \mathbf{p}_0, \mathbf{p}_1, \dots, \mathbf{p}_n$  be the intermediate waypoints from start to goal pose and  $l_i = \langle \mathbf{p}_i, \mathbf{p}_{i+1} \rangle$  be the  $i^{\text{th}}$  line segment, where  $i = 1, \dots, n - 1$ . Each line segment constitutes convex polyhedra, namely,  $E_i$ . Along with that, SFC can be expressed as  $SFC(P) = \{E_i \mid i = 0, \dots, n - 1\}$ . 360 SFC has two steps: finding  $E_i$  that fits the  $l_i$  and seeking a set of linear inequalities that are tangent to  $E_i$ . Let  $E_i$  be  $\varepsilon_i(C_i, \mathbf{p}_i^0) = \{\mathbf{p} = C_i\tilde{\mathbf{p}} + \mathbf{p}_i^0 \mid \|\tilde{\mathbf{p}}\|_2 \leq 1\}$ . In  $\mathbb{R}^3$ ,  $C_i$  can be decomposed as  $R^T S R$ , where R gives the axis of rotation between considered line segment in between  $\mathbf{p}_i$  and  $\mathbf{p}_{i+1}$ . Semi-axis of  $E_i$  is given by  $S = \operatorname{diag}(a, b, c)$  as a diagonal matrix.  $\mathbf{p}_i^0$  is the center of  $l_i$ . The objective of 365 SFC is to find each pair  $E_i$  and  $\mathbf{p}_i^0$ , given the  $l_i$  and obstacles set ( $Obs_i$ ), which touches the  $E_i$ .

Initially, ellipsoids are spheres whose center poses are located as the mid-



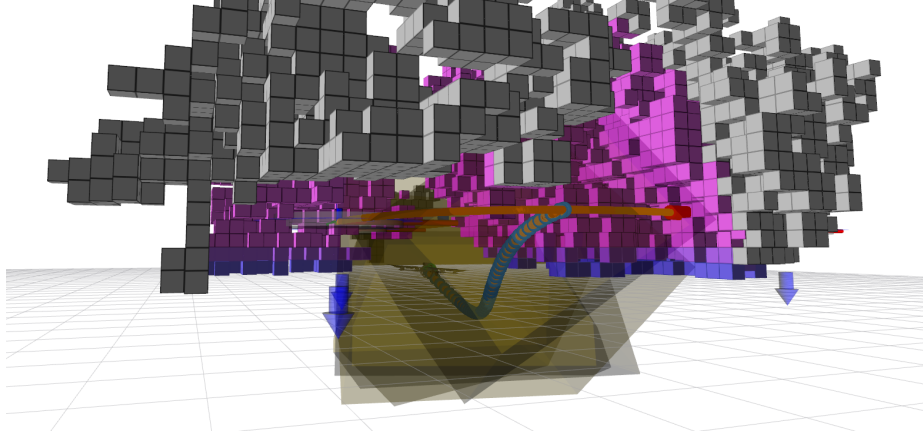


Figure 9: Free space extraction using SFC. Once intermediate initial waypoints are defined, SFC calculates free space along the path, which is constructed from the initial waypoints

points of  $l_i$ ,  $i = 1, \dots, n - 1$ . Afterwards, semi-axes except for the axis along  $\mathbf{p}_{i+1} - \mathbf{p}_i$ , are shrunk until the corresponding ellipsoid contains no obstacles. Let  $\varepsilon_i^*(C_i, \mathbf{p}_i^0)$  be the  $i$ th ellipsoid after applying the shrinking process.  $\mathbf{p}_j$  denotes the closest point that touches the  $\varepsilon_i^*(C_i, \mathbf{p}_i^0)$ , where  $j = 1, \dots, m$  and  $m$  is the number of obstacles. Hence, corresponding half-space  $H_j = \{\mathbf{p}_j \mid \mathbf{a}_j^T \mathbf{p}_j < \mathbf{b}_j\}$  is defined as a plane that is tangential to  $\varepsilon_i^*(C_i, \mathbf{p}_i^0)$ , where  $\mathbf{a}_j$  and  $\mathbf{b}_j$  are determined by:

$$\mathbf{a}_j = \frac{d\varepsilon_i}{d\mathbf{p}}_{\mathbf{p}=\mathbf{p}_j} = 2C_i^{-1}C_i^{-T}(\mathbf{p}_j - \mathbf{p}_i^0), \quad \mathbf{b}_j = \mathbf{a}_j^T \mathbf{p}_j. \quad (40)$$

Hence, the intersections of these  $m$  half spaces create a convex polyhedron  $C = \cup_{j=0}^m H_j = \{\mathbf{p} \mid A^T \mathbf{p} < \mathbf{b}\}$ . The same approach is applied to each line segment,  $l_i$  in which we can generate each  $C_i$ . All in all,  $SFC(P) = \{C \mid i = 0, \dots, n - 1\}$  can be constructed. A more descriptive formulation is in [17, Algorithm 1].

370

## 6. Continuous Trajectory Refinement

The objective function consists of several sub-objective functions: for improving the smoothness, for avoiding obstacles and so forth. In this section,

a precise explanation is given on how to construct sub-objective functions for each of the various occasions. First, we examine the simplest case where only dynamic feasibility and obstacle avoidance constraints are taken into consideration. Let  $J$  be the objective function or performance index

$$J(\Gamma) = \xi_{smooth} J_{smooth}(\Gamma) + \xi_{obs} J_{obs}(\Gamma). \quad (41)$$

There are various formulations of how  $J_{obs}$  and  $J_{smooth}$  are determined. In general,  $J_{smooth}$  can be expressed as:

$$J_{smooth}(\Gamma) = \frac{1}{2} \int_0^1 \left\| \frac{d\Gamma(t)}{dt} \right\|^2 dt. \quad (42)$$

Eliminating unnecessary higher-order motion is the main objective of the  $J_{smooth}$ . On the other hand,  $J_{obs}$  encourages to generate or modify collision-free trajectory by trying to push control points away from the obstacle zone if the trajectory is already in collisions or penalizing parts of the trajectory that is close to the obstacles. Let  $B \subset \mathbb{R}^d$  be the exterior boundary of the MAV and  $c$  is the cost function of penalizing close-in obstacles with respect to B. Along with that,  $J_{obs}$  can be formulated as follows:

$$J_{obs}(\Gamma) = \int_0^1 \int_{u \in B} c(f_c(\Gamma(t), \mathbf{p})) \left\| \frac{df_c(\Gamma(t), \mathbf{p})}{dt} \right\|^2 d\mathbf{p} dt, \quad (43)$$

where the function  $f_c(\Gamma(t), \mathbf{p})$ , which was proposed by Ratliff at al. [27], can be defined as follows:

$$f_c(\Gamma(t), \mathbf{p}) = \begin{cases} -dis(\Gamma(t), \mathbf{p}) + \frac{1}{2}\delta_{dis} & \text{if } dis(\Gamma(t), \mathbf{p}) < 0 \\ \frac{1}{2\delta_{dis}}(dis(\Gamma(t), \mathbf{p}) - \delta_{dis})^2 & \text{if } 0 < dis(\Gamma(t), \mathbf{p}) \leq \delta_{dis} \\ 0 & \text{otherwise} \end{cases}, \quad (44)$$

where  $\delta_{dis}$  denotes the distance from the boundary (B) of the quadrotor to a given obstacle position. Before taking gradient at  $i$ ,  $J(\Gamma)$  is linearized around  $i$ ,  $J(\Gamma) \approx J(\Gamma_i) + (\Gamma - \Gamma_i)^T \nabla J(\Gamma_i)$ . Defining  $c$  and  $d$  is detailed in [27, eqs.(22-28)].

In [21], the cost of the trajectory was estimated based on the following formulation:

$$J(\Gamma) = \xi_{obs} J_{obs}(\Gamma) + \xi_{smooth} J_{smooth}(\Gamma) + \xi_{soft} J_{soft}(\Gamma), \quad J_{soft}(\Gamma) = J_v(\Gamma) + J_a(\Gamma), \quad (45)$$

where  $J_{soft}(\Gamma)$  is determined by soft limits on acceleration and velocity.  $J_{smooth}(\Gamma)$  is defined by considering only geometric information without minimizing snap and/or jerk [3]. Such minimization is required because of the following stages of trajectory optimization. In such trajectory optimization, time reallocation has less impact on the objective function. Hence,  $J_{smooth}(\Gamma)$  is defined as follows:

$$J_{smooth}(\Gamma) = \sum_{i=d-1}^{n+1-d} \left\| \underbrace{\mathbf{p}_{i+1} - \mathbf{p}_i}_{f_{i+1,i}} + \underbrace{\mathbf{p}_{i-1} - \mathbf{p}_i}_{f_{i-1,i}} \right\|^2, \quad (46)$$

375 where a number of control points, denoted  $n$ , and  $\mathbf{f}_{i+1,i}$  and  $\mathbf{f}_{i-1,i}$  can be interpreted as connecting joint force of two springs between control points pairs:  $(\mathbf{p}_{i+1}, \mathbf{p}_i)$  and  $(\mathbf{p}_{i-1}, \mathbf{p}_i)$ , for example, control points lie on a straight line if the sum of all terms equals zero. As aside, similar approaches were proposed in [91, 92].

The value of  $J_{obs}(\Gamma)$  is determined by calculating the distance to the closest object pose from each control point in which the distance to the obstacle, i.e.,  $f_c(\mathbf{p}_i)$ , is given by

$$f_c(\mathbf{p}_i) = \begin{cases} (dis(\mathbf{p}_i) - \delta)^2 & dis(\mathbf{p}_i) \leq \delta_{dis} \\ 0 & dis(\mathbf{p}_i) > \delta_{dis} \end{cases}, \quad (47)$$

where  $\delta_{dis}$  is the free distance between MAV's center and the pose of the closest obstacle. Hence,  $J_{obs}(\Gamma) = \sum_{i=d}^n f_c(\mathbf{p}_i)$  can be estimated based on a given trajectory in the form of control points. Soft constraints are defined by not exceeding both acceleration and velocity within those max limits.

$$J_v(\Gamma) = \sum_{\mu} \sum_{i=d-1}^{n-d} f_v(\mathbf{v}_{i,\mu}), \quad J_a(\Gamma) = \sum_{\mu} \sum_{i=d-2}^{k_d-d} f_a(\mathbf{a}_{i,\mu})$$

$$f(\mathbf{v}) = \begin{cases} (\mathbf{v}_{\mu}^2 - \mathbf{v}_{max}^2)^2 & \mathbf{v}_{\mu}^2 > \mathbf{v}_{max}^2 \\ 0 & \mathbf{v}_{\mu}^2 \leq \mathbf{v}_{max}^2 \end{cases}, \quad f(\mathbf{a}) = \begin{cases} (\mathbf{a}_{\mu}^2 - \mathbf{a}_{max}^2)^2 & \mathbf{a}_{\mu}^2 > \mathbf{a}_{max}^2 \\ 0 & \mathbf{a}_{\mu}^2 \leq \mathbf{a}_{max}^2 \end{cases}, \quad (48)$$

To calculate acceleration and velocity at each control point and when both acceleration and velocity exceed their maximum limits, convex hull property (33) of b-spline is utilized to penalize those control points. Based on the previous

method, [26] proposed an endpoint cost  $J_{endpoint}(\Gamma)$ , into the objective function as an additional term. The key intuition behind adding  $J_{endpoint}(\Gamma)$  is to reduce the error between local trajectory and global trajectory since  $J_{endpoint}(\Gamma)$  penalizes error of both velocity and position with respect to the desired global trajectory.  $J_{endpoint}(\Gamma)$  is determined as follows:

$$J_{endpoint}(\Gamma) = J_{end}(\Gamma) = \xi_{end}^p(\mathbf{p}(t_{end}) - \mathbf{p}_{end})^2 + \xi_{end}^v(\dot{\mathbf{p}}(t_{end}) - \dot{\mathbf{p}}_{end})^2, \quad (49)$$

where  $\xi_{end}^p$  and  $\xi_{end}^v$  are regularization parameters, whereas  $\mathbf{p}_{end}$  and  $\dot{\mathbf{p}}_{end}$  are desired end position and velocity of the trajectory.

## 7. Receding Horizon Trajectory Planning

On most occasions, paths which are obtained by planning techniques are sub-optimal. Hence, the initial trajectory that is generated based on the initial path is to be refined, ensuring dynamic feasibility for controlling the MAV. Various approaches can be applied for trajectory refinement. However, enabling recursive feasibility, incorporating terminal constraints and convergence to the desired state are the utmost importance considerations to be contemplated throughout the process. LQR and MPC are the two most popular approaches that are being used for receding horizon planning. LQR is applied for linear systems, whereas iLQR and DDP are applied for non-linear system. Both in LQR or iLQR, OCP is defined as an open-loop control problem. On the other hand, MPC is designed as a close-loop OCP. In other words, OCP is seeking actions knowing the behaviour of the surrounding environment.

### 7.1. LQR based trajectory generation

DDP [93, 94] is one of the first techniques proposed for solving optimal control problems. Let  $\mathbf{x}_{k+1} = \mathbf{f}_d(\mathbf{x}_k, \mathbf{u}_k)$  be the discrete-time system dynamics; the total cost of the trajectory can be formulated for a given control policy, i.e.,  $\pi_{k+i}$ , for all  $i = \{0, 1, \dots, N - 1\}$ .

$$\sum_{i=0}^{N-1} c(\mathbf{x}_{k+i}, \mathbf{u}_{k+i}) + c_{goal}(\mathbf{x}_{k+N}). \quad (50)$$

The optimal control input, i.e.,  $\mathbf{u}_{k+i} = \pi_{k+i}(\mathbf{x}_{k+i})$ , for a given time index, i.e.,  $i+k$ , can be obtained by minimizing the (50). Thus, cost (cost-to-go) which was proposed in [95] is fully determined by

$$V_{k+i}(\mathbf{x}_{k+i}) = \min_{\mathbf{u}_{k+i}} (c(\mathbf{x}_{k+i}, \mathbf{u}_{k+i}) + V_{k+1}(\mathbf{f}_d(\mathbf{x}_{k+i}, \mathbf{u}_{k+i}))). \quad (51)$$

The same procedure can be applied recursively in a backward direction for seeking the optimal  $\pi_{k+i}(\mathbf{x}_{k+i}) = \arg \min_{\mathbf{u}_{k+i}} (c(\mathbf{x}_{k+i}, \mathbf{u}_{k+i}) + V_{k+1}(\mathbf{f}_d(\mathbf{x}_{k+i}, \mathbf{u}_{k+i})))$ . DDP yields almost the same behaviour: first estimate optimal control and then apply a forward pass to determine the updated nominal trajectory. Consequently, LQR is a simplified version of DDP. LQR is one of the fundamental ways to obtain a closed-form solution for a given optimal control problem under which system dynamics is assumed to be linear. Let us assume the system dynamics is defined as in (4). The intuition of LQR is to estimate the optimal control sequence for maneuvering the quadrotor from an initial position to the desired pose. Let  $N$  be the receding horizon whose optimal trajectory is to be determined. The total cost, i.e.,  $J_k(\mathbf{x}_k, \pi_N)$ , consists of three parts: initial, intermediate and final costs, where  $\pi_N = \{\pi_k, \pi_{k+1}, \dots, \pi_{k+i}, \dots, \pi_{N-1}\}$

$$J_k(\mathbf{x}_k, \pi_N) = c_{start}(\mathbf{x}_k) + \sum_{i=0}^{N-1} c(\mathbf{x}_{k+i}, \mathbf{u}_{k+i})dt + c_{end}(\mathbf{x}_{k+N}), \quad (52)$$

where  $\frac{\partial^2 C_{start}(x_k)}{\partial x \partial x} \leq 0$ ,  $\frac{\partial^2 C_{goal}(x_{k+N})}{\partial x \partial x} \leq 0$ ,  $\frac{\partial^2 C}{\partial \begin{bmatrix} x \\ u \end{bmatrix} \partial \begin{bmatrix} x \\ u \end{bmatrix}} \leq 0$ , and  $\frac{\partial^2 C}{\partial u \partial u} \leq 0$

are positive semidefinite Hessians to guarantee the minimizing of the total cost.

The total cost can be formulated in various ways. In LQR, the total cost is

defined as Quadratic costs as follows:

$$\begin{aligned}
c_{start}(\mathbf{x}_k) &= \frac{1}{2} \mathbf{x}_k^T Q_{start} \mathbf{x}_k + \mathbf{x}_k^T q_{start}, \\
c_{goal}(\mathbf{x}_{k+N}) &= \frac{1}{2} \mathbf{x}_{k+N}^T Q_{goal} \mathbf{x}_{k+N} + \mathbf{x}_{k+N}^T q_{goal}, \\
c(\mathbf{x}_{k+i}, \mathbf{u}_{k+i}) &= \frac{1}{2} \mathbf{x}_{k+i}^T Q \mathbf{x}_{k+i} + \frac{1}{2} \mathbf{u}_{k+i}^T R \mathbf{u}_{k+i} + \mathbf{u}_{k+i}^T P \mathbf{x}_{k+i} + \mathbf{x}_{k+i}^T p \\
&+ \mathbf{u}_{k+i}^T r + \xi = \frac{1}{2} \begin{bmatrix} \mathbf{x}_{k+i} \\ \mathbf{u}_{k+i} \end{bmatrix}^T \underbrace{\begin{bmatrix} Q & P^T \\ P & R \end{bmatrix}}_{J_k} \begin{bmatrix} \mathbf{x}_{k+i} \\ \mathbf{u}_{k+i} \end{bmatrix} + \begin{bmatrix} \mathbf{x}_{k+i} \\ \mathbf{u}_{k+i} \end{bmatrix} \underbrace{\begin{bmatrix} p \\ r \end{bmatrix}}_{j_k} + \xi,
\end{aligned} \tag{53}$$

where  $i \in \{0, 1, \dots, N-1\}$ ,  $Q_{start} \in \mathbb{R}^{n_x \times n_x}$ ,  $Q_{goal} \in \mathbb{R}^{n_x \times n_x}$ ,  $Q \in \mathbb{R}^{n_x \times n_x}$ ,  $R \in \mathbb{R}^{n_u \times n_u}$ ,  $P \in \mathbb{R}^{n_u \times n_x}$ ,  $q_{start} \in \mathbb{R}^{n_x}$ ,  $q_{goal} \in \mathbb{R}^{n_x}$ ,  $p \in \mathbb{R}^{n_x}$ ,  $r \in \mathbb{R}^{n_u}$ , and  $\xi \in \mathbb{R}$  are predefined in which  $Q_{start}$ ,  $Q_{goal}$ ,  $Q$ , and  $R$  are positive definite, whereas  $J_k \geq 0$  and  $j_k \geq 0$  assumed to be positive semi-definite. LQR problem( 52) and (53) provides an optimal  $\pi_N$  in close form solution as expressed in 51; the cost-to-go function, i.e., 51, can be reformulated as an explicit quadratic formulation as follows:

$$V_{k+i}(\mathbf{x}_{k+i}) = \frac{1}{2} \begin{bmatrix} \mathbf{x}_{k+i} \\ \mathbf{u}_{k+i} \end{bmatrix}^T J_{k+i} \begin{bmatrix} \mathbf{x}_{k+i} \\ \mathbf{u}_{k+i} \end{bmatrix} + \begin{bmatrix} \mathbf{x}_{k+i} \\ \mathbf{u}_{k+i} \end{bmatrix}^T j_{k+i} + \xi. \tag{54}$$

Estimation of both  $J_{k+i}$  and  $j_{k+i}$  can be obtained in a recursive way starting from the goal position  $\mathbf{x}_{k+N}$  to the initial position  $\mathbf{x}_k$ , using Riccati differential equation for all  $i = \{0, \dots, N-1\}$ .

$$\begin{aligned}
J_k &= Q + A_k^T J_{k+1} A_k - \\
&(P + B_k^T J_{k+1} A_k)^T \cdot (R + B_k^T J_{k+1} B_k)^{-1} \cdot (P + B_k^T J_{k+1} A_k) \\
j_k &= p + A_k^T j_{k+1} + A_k^T J_{k+1} c_k \\
&- (P + B_k^T J_{k+1} A_k)^T \cdot (R + B_k^T J_{k+1} B_k)^{-1} \cdot (r + B_k^T j_{k+1} + B_k^T J_{k+1} c_k).
\end{aligned} \tag{55}$$

In general, system dynamics is described by:

$$\mathbf{x}_{k+1} = \mathbf{f}_d(\mathbf{x}_k, \mathbf{u}_k) = A_k \mathbf{x}_k + B_k \mathbf{u}_k, \tag{56}$$

. If the system dynamics is non-linear,  $A_k$  and  $B_k$  are recalculated by linearizing the  $\mathbf{f}_c$  at each time index. Since linearization has to be carried out in each

iteration, it is called the iLQR [28].

$$A_k = \frac{\partial \mathbf{f}_c}{\partial \mathbf{x}}(\mathbf{x}_k, \mathbf{u}_k), \quad B_k = \frac{\partial \mathbf{f}_c}{\partial \mathbf{u}}(\mathbf{x}_k, \mathbf{u}_k). \quad (57)$$

Boundary or goal position conditions are given by  $S_{k+N} = Q_{goal}$ ,  $j_{k+N} = q_{goal}$ . The feedback control policy in LQR is fully determined as follows:

$$\begin{aligned} \pi_k(\mathbf{x}_k) = & -(R + B_k^T J_{k+1} B_k)^{-1} \cdot (P + B_k^T J_{k+1} A_k) \mathbf{x}_k \\ & -(R + B_k^T J_{k+1} B_k)^{-1} \cdot (r + B_k^T j_{k+1} + B_k^T J_{k+1} B_k). \end{aligned} \quad (58)$$

As given in (55), system stability depends on system dynamics. When quadrotor dynamics is non-linear, the stability of iLQR is not guaranteed. Jur and Berg [29] attempted to address the stability issue by proposing a novel method called LQR smoothing; this method can be applied for linear or non-linear systems to acquire the minimum-cost trajectory. The main difference in LQR smoothing compared to LQR is that LQR minimizes the cost of not only backward direction, i.e., cost-to-go, but also applies forward direction, i.e., cost-to-come [29, 6, 96]. However, the output of LQR, iLQR or LQR smoothing does not address the system noise. Both linear or nonlinear state estimator may eliminate the system noise. LQG [30, 97] is one of the ways to solve this problem. LQG consists of a state estimator, i.e., Kalman Filter (KF), and state feedback, i.e., iLQR or LQR.

## 7.2. MPC based trajectory generation

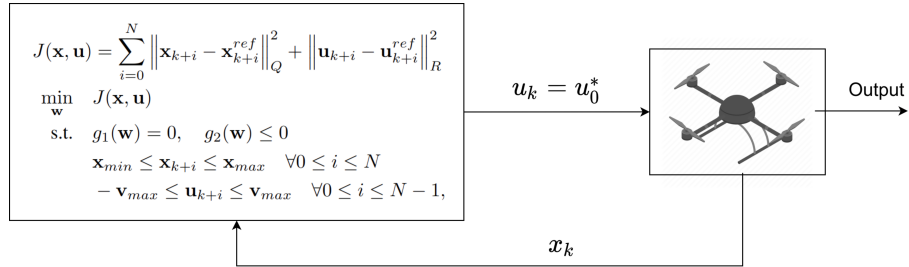


Figure 10: The basic idea of MPC-based receding horizon planning

As detailed in section 7.1, unaccountability of addressing sudden distur-  
410 bances is the main limitation of OCP techniques (e.g., LQR, DDP); this is due  
to its nature. LQR calculates fixed receding control policy and applies to the  
system; there is no intervention during the control policy execution. MPC is  
one of the ways to address the preceding problem, which is characteristic of  
both LQR and DDP. The difference between MPC and LQR is that only the  
415 first portion of the control policy is applied to system in MPC through the cal-  
culate of full control policy rather than employing full control policy as in LQR.  
Let us assume the system dynamics as given in (2). In general, MPC can be  
formed as follows:

$$\begin{aligned}
& \min_w J_{end}(\mathbf{x}_{k+N}, \mathbf{x}_{k+N}^{ref}) + J_k(\mathbf{x}, \mathbf{u}, \mathbf{x}^{ref}, \mathbf{u}^{ref}) \\
& \text{s.t. } \mathbf{x}_{k+1} = \mathbf{f}_d(\mathbf{x}_k, \mathbf{u}_k) \\
& \quad \mathbf{x}^{min} \leq \mathbf{x}_{k+i} \leq \mathbf{x}^{max} \quad \forall 0 \leq i \leq N \\
& \quad \mathbf{u}^{min} \leq \mathbf{u}_{k+i} \leq \mathbf{u}^{max} \quad \forall 0 \leq i < N - 1 \\
& \quad g_1(w) = 0 \\
& \quad g_2(w) \leq 0,
\end{aligned} \tag{59}$$

where  $w = \mathbf{u}_k, \dots, \mathbf{u}_{k+N-1}$  is the optimal control sequence to be estimated in each iteration. Variable  $J_{end}(\mathbf{x}_{k+N})$  plays a significant role in terms of the stability of the system locally and globally. Presenting local stability is relatively easy, e.g., Lyapunov's analysis compared to global stability. In addition to terminal cost, terminal constraints for states should be enforced, which is quite computationally challenging for real-time applications. Moreover, enforcing terminal constraints is even more difficult for non-linear dynamics. Thus, in most of the practical applications, terminal constraints are not enforced into the optimization procedure. Furthermore, classical MPC lacks recursive feasibility. Several varieties of MPC have been proposed to address processing issues to a certain extent. For a linear system, the performance index, i.e.,  $J_k(\mathbf{x}, \mathbf{u}, \mathbf{z}^{ref}, \mathbf{u}^{ref})$ , can



be defined as follows:

$$\begin{aligned}
& J_k(\mathbf{x}, \mathbf{u}, \mathbf{z}^{ref}, \mathbf{u}^{ref}) \\
= & \sum_{i=0}^{N-1} ((\mathbf{x}_{k+i} - \mathbf{x}_{k+i}^{ref})^T Q_x (\mathbf{x}_{k+i} - \mathbf{x}_{k+i}^{ref}) + (\mathbf{u}_{k+i} - \mathbf{u}_{k+i}^{ref})^T R_u (\mathbf{u}_{k+i} - \mathbf{u}_{k+i}^{ref})) \\
& + (\mathbf{x}_{k+N} - \mathbf{x}_{k+N}^{ref})^T P (\mathbf{x}_{k+N} - \mathbf{x}_{k+N}^{ref}), \tag{60}
\end{aligned}$$

where  $Q_x$ , which is a positive semi-definite matrix, consists of the state error penalty coefficients, whereas  $R_u$  should be positive definite and  $P$  is state error on the terminal cost. In principle, stability and feasibility are not assured implicitly. Consequently, stability and feasibility tend to improve for the longer receding horizon, which is quite challenging due to computational demands.

Quadrotor dynamics are usually expressed in a non-linear fashion. Therefore LQR or linear MPC can not be applied without linear approximation. Hence, Nonlinear Programming (NLP)-based approach has to be applied. Direct multiple shooting and direct collocation are the main two techniques that are used to transform OCP into NLP. In both direct multiple shooting and direct collocation, the state is minimized in addition to controlling inputs. Direct multiple shooting differs from direct collocation due to the way of the problem formulation. In multiple shooting, the problem is quantized into  $N$  subintervals, i.e., receding horizon length. In direct collocation, however, those subintervals are further described by a set of polynomials such as B-spline or Lagrangian; this will increase the problem sparsity. On the contrary, the number of optimization parameters to be optimized has dramatically increased in direct collocation compared to multiple shooting. This, collocation is better when it is accuracy-wise, but direct multiple shooting is better when it is performance-wise. In [71], the trajectory tracking problem is formulated based on direct collocation and multiple shooting. Further, the researchers have proved that multiple shooting has a lower computational footprint compared to direct collocation.

### 7.3. Disturbance Estimation

In the context of optimal trajectory planning, simultaneously computing optimal control policy, which is required to respond to unknown, sudden disturbances, and handling kinematics (i.e., obstacle avoidance) as well as dynamics (i.e., satisfying velocity and acceleration constraints) yields a challenging problem, especially for quadrotors. While geometry-based path planning techniques [98, 99] ensure the asymptotical optimality of a path, they however do not consider quadrotor dynamics. But, it is essential that the generation of an optimal control policy ensures dynamic feasibility. So, in [100, 101], LQR was incorporated into path planning, by which both dynamic feasibility and local optimality were guaranteed. However, local optimality does not necessarily yield global optimality [102]. In [17, 14], a set of motion primitives was used to find feasible trajectories ensuring both global and local optimality. When dealing with unknown disturbances, MPC is a more robust technique than LQR. In [17], MPC-based trajectory planning approach was proposed, ensuring both the local and global optimality. However, none of the aforesaid approaches formally guarantees stability and safety. Lyapunov’s analysis can be applied to confirm the local stability. Moreover, the terminal constraints set [103] can be incorporated. However, those measures are time-consuming, which directly affects the real-time performance [104]. A set of CBFs was proposed for improving real-time performance without affecting the system stability in [105, 106, 33]. Recently, reference governors-based techniques were proposed in [107, 108], enforcing safety constraints. It is natural that designing a path planner is followed by the actual controller to maneuver MAV. In such approaches, a reference governor can be used to handle the stability and constraint satisfaction separately to ensure system stability [109].

The above approaches are employed to estimate optimal control policy for safe navigation while imposing stability either using Lyapunov functions or reference governors. On the other hand, Li et al. [110] proposed to obtain an optimal control policy using a State-dependant Distance Metric (SDDM). They

have modelled the system dynamics as a linear, time-invariant as follows:

$$\dot{\mathbf{x}} = A\mathbf{x} + B\mathbf{u}, \quad (61)$$

where  $\mathbf{u}$  indicates the control input. System state, i.e.,  $\mathbf{x} := (\mathbf{p}(t), \mathbf{y}(t))$ , consists of two parts:  $\mathbf{p}$  and  $\mathbf{y}$ , where  $\mathbf{p}(t)$  denotes the quadrotor position at a given time  $t$  and  $\mathbf{y}(t)$  describes the higher-order terms, e.g., velocity, acceleration, etc. In the latter work, the quadratic norm was utilized to represent the error between robot position and close-in obstacles positions. The quadratic norm is defined as  $\|\mathbf{p}\|_R := \sqrt{\mathbf{p}^T R \mathbf{p}}$ , where  $R$  is a symmetric positive matrix.  $R[\psi_z]$  is fully determined by the MAV heading direction  $\psi_z$  at a given time instance as follows:

$$R[\psi_z] = \begin{cases} c_2 I + (c_1 - c_2) \frac{\psi_z \psi_z^T}{\|\psi_z\|^2}, & \text{if } \psi_z \neq 0 \\ c_1 I, & \text{otherwise} \end{cases}, \quad (62)$$

where both  $c_1$  and  $c_2$  are predefined scales such that  $c_2 > c_1 > 0$ ; this process is called the SDDM, trajectory will be bounded incorporating SDDM information. Since quadrotor dynamics is linear, a reference governor [108] is introduced to maintain safety and stability. Other than LQR and MPC, there exist several receding horizon-based techniques for optimal trajectory planning as given in Table 2.

## 8. Solving Trajectory Planning Problem

As explained in the preceding sections, several constraints (e.g., soft and hard) are imposed to ensure dynamic feasibility, smooth navigation, handling disturbances, etc. Hence, optimal trajectory planning is posed as a constraint optimization problem in most situations. Constraint-based optimization problems are solved in two different ways: adding hard constraints or introducing soft constraints. In general, a constraint-based optimization problem can be formulated as a quadruple, i.e.,  $P_{constraint} = (c, g1, g2, J)$ , where  $c$  stands for performance index or cost function, whereas equality and inequality constraints

Table 2: Comparison of properties of receding horizon trajectory planning techniques

Algorithm	Motion Model		Gradient Estimator	
	Linear	Nonlinear	Hamiltonian	Gradient
Differential Dynamic Programming (DDP) [111]	✗	✓	✗	✓
Linear Quadratic Regulator (LQR) [112]	✓	✗	✗	✗
Iterative LQR (iLQR) [113]	✗	✓	✗	✓
Linear Model Predictive Control (MPC) [114]	✓	✗	✗	✗
Nonlinear Model Predictive Control (NMPC) [71]	✓	✓	✓	✗
Constrained Nonlinear Model Predictive Control CGMRES (NMPC-CGMRES) [115]	✗	✓	✓	✗
Corridor-based Model Predictive Contouring Control(CMPCC) [32]	✓	✗	✗	✗
Constrained Nonlinear Model Predictive Control Newton (NMPC-Newton) [116]	✗	✓	✗	✗
Model Preidictive Path Integral Control (MPPI) [117]	✓	✓	✗	✗
Cross Entropy Method (CEM) [118]	✓	✓	✗	✗

490 are given by  $g_1$  and  $g_2$ , respectively. The objective function is given by  $J$ . In  
hard constraint-based formulation, the optimal solution, i.e.,  $\mathbf{w}$ , for  $P_{constraint}$   
is calculated, ensuring all the constraints. In soft constraints formulation, the  
objective function does not need to satisfy all the constraints, but satisfying  
those constraints will improve the final  $\mathbf{w}$ . D. Mellinger and V.Kumar [3] took  
495 the lead in proposing a successful approach for trajectory generation as a hard  
constraint-based optimization approach, i.e., Minimum-snap. Subsequently,  
in [51], the researchers extended the Minimum-snap trajectory generation as  
an unconstrained or soft constraint-based optimization problem.

When generating trajectories, ensuring a collision-free path is essential. Hence,  
500 representing free space in a structured way and imposing obstacle constraints  
for trajectory generation is a must for safety. Free space can be represented  
in different ways such as cubes ([13, 14]), spheres ([15, 16]) and polyhedrons  
([17]). The intuition of these approaches is to apply path planning through the  
free space to obtain the intermediate waypoints. Once intermediate waypoints  
505 are extracted, the trajectory generation procedure is utilised for retrieving a  
smooth, feasible, collision-free trajectory. On the other hand, in [47, 24, 14],  
kinodynamic path planning followed by B-spline-based trajectory generation is  
considered. Most of the works that were proposed for soft constraint-based  
trajectory generation formulated optimal trajectory planning as nonlinear op-  
510 timization problems in which smoothness and safety were introduced as soft  
constraints. Most of the time gradient-descent based [63] or gradient-free ap-  
proaches [66, 53] were applied for minimizing the cost of smoothness and safety.

The constraints optimization problem can be designed in either QP or NLP  
form. In QP, the procedure is to minimize or maximize the objective subject to  
515 a set of linear constraints in most situations. On the other hand, non-quadratic  
programming is used to handle the non-linear constraints each of which has a  
unique nature to solve the problem. In general, QP objective can be described

as:

$$\begin{aligned} \min_{\mathbf{x}} \quad & \frac{1}{2} \mathbf{x}^T Q \mathbf{x} + c^T \mathbf{x} \\ \text{s.t.} \quad & A \mathbf{x} \succeq b, \end{aligned} \tag{63}$$

where  $A \mathbf{x} \succeq b$  stands for the set of linear inequalities.  $Q$  is a positive symmetric matrix. There are various ways to solve QP, including interior point, active set and gradient projection. In some situations, multiple variables that are to be optimized are integer values; those are solved as MIQP. For example, FASTER [119] used MIQP for safe trajectory planning with aggressive controls [52].

Most of the recent optimal trajectory planning techniques [21, 26, 20, 53] were formulated as GTO in which optimization problem was designed as a non-linear form. The gradient descent is performed with respect to each parametrization index of  $\Gamma$  to minimize the different, i.e.,  $\Gamma_{i+1} - \Gamma_i$ . Hence,  $\Gamma_{i+1}$  can be determined by solving the following optimization problem as given in [120, 63].

$$\Gamma_{i+1} = \arg \min_{\Gamma} J(\Gamma_i) + (J(\Gamma) - J(\Gamma_i))^T \nabla J(\Gamma_i) + \frac{\eta}{2} \|\Gamma - \Gamma_i\|_M^2, \tag{64}$$

where  $M$  is a weighting matrix and  $\eta$  is a regularization parameter. GTO is rather popular due to its ability to deform infeasible trajectory segments, low memory requirement and high throughput. Despite having the listed advantages, GTO can not avoid the problem of a local minimum. STOMP [66] is one of the early techniques proposed to address the local minimum problem. STOMP is based on the gradient-free technique. However, STOMP is unable to obtain real-time performance. Besides STOMP, the local minimum problem has been addressed by various recent works. Yet, this remains an open problem to be solved. Zhou [121] proposed a method, i.e., Path-guided Optimization (PGO), for overcoming local minima problem by generating topologically distinct paths and doing parallel optimization. Furthermore, various solvers can be utilized for solving optimization problems, including BOBYQA [122], L-BFGS [123, 11], ACADO [124], SLSQP [125], Proximal

Operator Graph Solver (POGS) [126, 127], Sequential Quadratic Programming (SQP) and MMA [128]. Shravan et al. [74] proposed a trajectory optimization technique in a distributed setup in which the researchers evaluated their  
540 formulation with several solvers. According to their observations, BOBYQA is faster compared to BFGS and SLSQP, while MMA yielded a similar performance to that of BOBYQA. In [129], L-BFGS was proposed for finding the shortest path in real-time; in this research effort however L-BFGS does not  
545 guarantee optimality, only feasibility is enforced. Mathematical Program with Complementarity Constraints (MPCC) [130] yet another proposed method for fast trajectory optimization in real-time. Moreover, Mathieu and Nicolas [131] proposed a SQP-based trajectory generation approach for carrying augmented loads. The intuition behind selecting SQP over other solvers is due to its super-  
550 linear convergency and ability to handle non-linear constraints within milliseconds.

## 9. Conclusion

All in all, we have thoroughly reviewed the trajectory planning problem in the paradigm of plan-based control for MAVs. Such trajectory planning  
555 problem was broken down into a set of subproblems: free-space segmentation, motion model selection, initial waypoints identification, initial trajectory generation, continuous trajectory refinement, and receding horizon trajectory planning. Afterwards, for each subproblem, we examined how previous research has addressed those by presenting and evaluating various approaches to the considered subproblem. Finally, several selected recent approaches were listed  
560 (Table 3) according to the listed subproblems we have identified. With that, we concluded that the trajectory planning problem can be designed by addressing those subproblems carefully for MAVs.

Approach	Dynamics Model (Exact/Empirical Differential flatness (DF))	Intermediate Waypoint Selection	Initial Trajectory Generation	Continuous trajectory refinement and solver	Free space extraction	Receding horizon planning or controlling
[121]	DF	Sampling-based topological search	PGO based B-splines	GTO	ESDF	-
[47]	DF	Kinodynamic-based search	B-splines	EO using QCQP	ESDF	-
[104]	DF	Kinodynamic-based search	Linear Quadratic Minimum Time	unconstrained QP	[132]	RHC
[53]	DF	Informed-RRT*	Continuous time polynomial	BFGS	ESDF	-
[40]	DF	-	Piecewise Bézier-based curve with minimum-jerk	Elastic band optimization	Convex Cluster	-
[21]	DF	A* kinodynamic search	B-splines	NLept [133]	ESDF	GTC
[24]	DF	B-spline kinodynamic search	EO	~QCQP	TSDF	-
[63]	DF	-	CHOMP	Functional gradient [120]	ESDF	CHOMP
[134]	DF	A*	uniform B-spline	BFGS, L-BFGS, T-NEWTON [135]	ESDF	-
[14]	DF	fast marching-based search	Bernstein polynomial	Mosek [136]	TSDF	-
[15]	DF	RRG combined with A*	piecewise polynomials	QCQP	KD-tree	GTC
[29]	Exact	line search	Iterated LQR Smoothing	Iterated LQR Smoothing	-	-
[49]	Exact	A*	Visual-Inertial Navigation System (VINS)	Gradient-based	TSDF	GTC
[86]	DF	RRT*	Uniform-Bspline	MMA and BFGS	OctoMap and Circular Buffer	GTC
[17]	DF	JPS	Minimum-span	Constrained QP	SFC	RHC
[110]	Empirical	piecewise-linear path	SDDM	SDDM	Constrained QP	-
[119]	DF	JPS	Cubic Bézier curve	MIQP using Gurobi [137]	SFC	-
[32]	Empirical	-	CMPC	OSQP [138]	SFC	RHC
[70]	Empirical	-	NMPC	ACADO [124]	-	MHE
[139]	Empirical	-	NMPC	SQP	-	RHC
[13]	DF	A*	Multi-segment polynomial	OOQP [140]	OctoMap	GTC
[51]	Exact	RRT*	Minimum-Span	Unconstrained QP	OctoMap	GTC
[141]	DF	MINVO basis [142]	Uniform B-spline	Augmented Lagrangian [143]	Outer polyhedral	-
[55]	DF	Piecewise linear path	Piecewise polynomial	MIQP using Mosek	IRIS	-
[144]	DF	Non-uniform kinodynamic search	Uniform B-spline	Constrained QP	ESDF	RHC
[71]	Empirical	Uniform B-spline	NMPC	CasADi[145] with Ipopt[146]	ESDF	PID



565 **References**

- [1] Pixhawk 4, <https://dev.px4.io/v1.9.0> (2020).
- [2] Dji, <https://www.dji.com/> (2020).
- [3] D. Mellinger, V. Kumar, Minimum snap trajectory generation and control for quadrotors, in: 2011 IEEE International Conference on Robotics and Automation, IEEE, 2011, pp. 2520–2525.
- [4] S. Ramasamy, G. Wu, K. Sreenath, Dynamically feasible motion planning through partial differential flatness., in: Robotics: Science and Systems, 2014.
- [5] T. R. Wanasinghe, G. K. Mann, R. G. Gosine, Relative localization approach for combined aerial and ground robotic system, *Journal of Intelligent & Robotic Systems* 77 (1) (2015) 113–133.
- [6] J. van den Berg, Extended lqr: Locally-optimal feedback control for systems with non-linear dynamics and non-quadratic cost, in: Robotics Research, Springer, 2016, pp. 39–56.
- [7] R. Deits, R. Tedrake, Computing large convex regions of obstacle-free space through semidefinite programming, in: Algorithmic foundations of robotics XI, Springer, 2015, pp. 109–124.
- [8] Y. Ling, S. Shen, Building maps for autonomous navigation using sparse visual slam features, in: 2017 IEEE/RSJ International Conference on Intelligent Robots and Systems (IROS), IEEE, 2017, pp. 1374–1381.
- [9] S. Savin, An algorithm for generating convex obstacle-free regions based on stereographic projection, in: 2017 International Siberian Conference on Control and Communications (SIBCON), IEEE, 2017, pp. 1–6.
- [10] X. Zhong, Y. Wu, D. Wang, Q. Wang, C. Xu, F. Gao, Generating large convex polytopes directly on point clouds, arXiv preprint arXiv:2010.08744.

- 595 [11] G. Kulathunga, H. Hamed, D. Devitt, A. Klimchik, Optimization-based trajectory tracking approach for multi-rotor aerial vehicles in unknown environments, *IEEE Robotics and Automation Letters* 7 (2) (2022) 4598–4605.
- [12] J. L. Bentley, Multidimensional binary search trees used for associative searching, *Communications of the ACM* 18 (9) (1975) 509–517.
- [13] J. Chen, K. Su, S. Shen, Real-time safe trajectory generation for quadrotor flight in cluttered environments, in: 2015 IEEE International Conference on Robotics and Biomimetics (ROBIO), IEEE, 2015, pp. 1678–1685.
- 600 [14] F. Gao, W. Wu, Y. Lin, S. Shen, Online safe trajectory generation for quadrotors using fast marching method and bernstein basis polynomial, in: 2018 IEEE International Conference on Robotics and Automation (ICRA), IEEE, 2018, pp. 344–351.
- 605 [15] F. Gao, S. Shen, Online quadrotor trajectory generation and autonomous navigation on point clouds, in: 2016 IEEE International Symposium on Safety, Security, and Rescue Robotics (SSRR), IEEE, 2016, pp. 139–146.
- [16] F. Gao, W. Wu, W. Gao, S. Shen, Flying on point clouds: Online trajectory generation and autonomous navigation for quadrotors in cluttered environments, *Journal of Field Robotics* 36 (4) (2019) 710–733.
- 610 [17] S. Liu, M. Watterson, K. Mohta, K. Sun, S. Bhattacharya, C. J. Taylor, V. Kumar, Planning dynamically feasible trajectories for quadrotors using safe flight corridors in 3-d complex environments, *IEEE Robotics and Automation Letters* 2 (3) (2017) 1688–1695.
- 615 [18] A. Stentz, Optimal and efficient path planning for partially known environments, in: *Intelligent unmanned ground vehicles*, Springer, 1997, pp. 203–220.

- 620 [19] I. Noreen, A. Khan, Z. Habib, A comparison of rrt, rrt\* and rrt\*-smart path planning algorithms, *International Journal of Computer Science and Network Security (IJCSNS)* 16 (10) (2016) 20.
- [20] F. Gao, Y. Lin, S. Shen, Gradient-based online safe trajectory generation for quadrotor flight in complex environments, in: *2017 IEEE/RSJ International Conference on Intelligent Robots and Systems (IROS)*, IEEE, 2017, pp. 3681–3688.
- 625 [21] B. Zhou, F. Gao, L. Wang, C. Liu, S. Shen, Robust and efficient quadrotor trajectory generation for fast autonomous flight, *IEEE Robotics and Automation Letters* 4 (4) (2019) 3529–3536.
- [22] D. J. Webb, J. Van Den Berg, Kinodynamic rrt\*: Asymptotically optimal motion planning for robots with linear dynamics, in: *2013 IEEE International Conference on Robotics and Automation*, IEEE, 2013, pp. 630 5054–5061.
- [23] R. Allen, M. Pavone, A real-time framework for kinodynamic planning with application to quadrotor obstacle avoidance, in: *AIAA Guidance, Navigation, and Control Conference*, 2016, p. 1374.
- 635 [24] W. Ding, W. Gao, K. Wang, S. Shen, An efficient b-spline-based kinodynamic replanning framework for quadrotors, *IEEE Transactions on Robotics* 35 (6) (2019) 1287–1306.
- [25] G. Rousseau, C. S. Maniu, S. Tebbani, M. Babel, N. Martin, Minimum-time b-spline trajectories with corridor constraints. application to cinematographic quadrotor flight plans, *Control Engineering Practice* 89 640 (2019) 190–203.
- [26] V. Usenko, L. von Stumberg, A. Pangercic, D. Cremers, Real-time trajectory replanning for mavs using uniform b-splines and a 3d circular buffer, in: *2017 IEEE/RSJ International Conference on Intelligent Robots and Systems (IROS)*, IEEE, 2017, pp. 215–222. 645

- [27] N. Ratliff, M. Zucker, J. A. Bagnell, S. Srinivasa, Chomp: Gradient optimization techniques for efficient motion planning, in: 2009 IEEE International Conference on Robotics and Automation, IEEE, 2009, pp. 489–494.
- [28] W. Li, E. Todorov, Iterative linear quadratic regulator design for nonlinear biological movement systems., in: ICINCO (1), 2004, pp. 222–229.
- [29] J. van den Berg, Iterated lqr smoothing for locally-optimal feedback control of systems with non-linear dynamics and non-quadratic cost, in: 2014 American Control Conference, IEEE, 2014, pp. 1912–1918.
- [30] E. Todorov, General duality between optimal control and estimation, in: 2008 47th IEEE Conference on Decision and Control, IEEE, 2008, pp. 4286–4292.
- [31] T. Nägele, J. Alonso-Mora, A. Domahidi, D. Rus, O. Hilliges, Real-time motion planning for aerial videography with dynamic obstacle avoidance and viewpoint optimization, IEEE Robotics and Automation Letters 2 (3) (2017) 1696–1703.
- [32] J. Ji, X. Zhou, C. Xu, F. Gao, Cmpcc: Corridor-based model predictive contouring control for aggressive drone flight, arXiv preprint arXiv:2007.03271.
- [33] A. D. Ames, X. Xu, J. W. Grizzle, P. Tabuada, Control barrier function based quadratic programs for safety critical systems, IEEE Transactions on Automatic Control 62 (8) (2016) 3861–3876.
- [34] A. Romero, R. Penicka, D. Scaramuzza, Time-optimal online replanning for agile quadrotor flight, arXiv preprint arXiv:2203.09839.
- [35] Z. Wang, X. Zhou, C. Xu, F. Gao, Geometrically constrained trajectory optimization for multicopters, IEEE Transactions on Robotics.
- [36] S. Upadhyay, T. Richardson, A. Richards, Generation of dynamically feasible window traversing quadrotor trajectories using logistic curve, Journal of Intelligent & Robotic Systems 105 (1) (2022) 1–17.

- [37] G. Torrente, E. Kaufmann, P. Foehn, D. Scaramuzza, Data-driven mpc  
675 for quadrotors, *IEEE Robotics and Automation Letters*.
- [38] L. Tang, H. Wang, Z. Liu, Y. Wang, A real-time quadrotor trajectory planning framework based on b-spline and nonuniform kinodynamic search, *Journal of Field Robotics* 38 (3) (2021) 452–475.
- [39] H. Heidari, M. Saska, Trajectory planning of quadrotor systems for various  
680 objective functions, *Robotica* 39 (1) (2021) 137–152.
- [40] F. Gao, L. Wang, B. Zhou, X. Zhou, J. Pan, S. Shen, Teach-repeat-replan: A complete and robust system for aggressive flight in complex environments, *IEEE Transactions on Robotics*.
- [41] T. Lee, M. Leok, N. H. McClamroch, Geometric tracking control of a  
685 quadrotor uav on se (3), in: 49th IEEE conference on decision and control (CDC), IEEE, 2010, pp. 5420–5425.
- [42] V. Zinage, S. H. Arul, D. Manocha, 3d-ogse: Online smooth trajectory generation for quadrotors using generalized shape expansion in unknown 3d environments, arXiv preprint arXiv:2005.13229.
- [43] L. Xi, Z. Peng, L. Jiao, Trajectory generation for quadrotor while tracking  
690 a moving target in cluttered environment, in: 2020 39th Chinese Control Conference (CCC), IEEE, 2020, pp. 6792–6797.
- [44] L. Han, F. Gao, B. Zhou, S. Shen, Fiesta: Fast incremental euclidean  
695 distance fields for online motion planning of aerial robots, arXiv preprint arXiv:1903.02144.
- [45] V. Murali, I. Spasojevic, W. Guerra, S. Karaman, Perception-aware trajectory generation for aggressive quadrotor flight using differential flatness, in: 2019 American Control Conference (ACC), IEEE, 2019, pp. 3936–3943.

- 700 [46] A. Abadi, A. El Amraoui, H. Mekki, N. Ramdani, Optimal trajectory generation and robust flatness-based tracking control of quadrotors, *Optimal Control Applications and Methods* 40 (4) (2019) 728–749.
- [47] W. Ding, W. Gao, K. Wang, S. Shen, Trajectory replanning for quadrotors using kinodynamic search and elastic optimization, in: *2018 IEEE International Conference on Robotics and Automation (ICRA)*, IEEE, 2018, pp. 7595–7602.
- 705 [48] F. Blochliger, M. Fehr, M. Dymczyk, T. Schneider, R. Siegwart, Topomap: Topological mapping and navigation based on visual slam maps, in: *2018 IEEE International Conference on Robotics and Automation (ICRA)*, IEEE, 2018, pp. 1–9.
- 710 [49] Y. Lin, F. Gao, T. Qin, W. Gao, T. Liu, W. Wu, Z. Yang, S. Shen, Autonomous aerial navigation using monocular visual-inertial fusion, *Journal of Field Robotics* 35 (1) (2018) 23–51.
- [50] C. Rösmann, F. Hoffmann, T. Bertram, Integrated online trajectory planning and optimization in distinctive topologies, *Robotics and Autonomous Systems* 88 (2017) 142–153.
- 715 [51] C. Richter, A. Bry, N. Roy, Polynomial trajectory planning for aggressive quadrotor flight in dense indoor environments, in: *Robotics Research*, Springer, 2016, pp. 649–666.
- 720 [52] B. Landry, R. Deits, P. R. Florence, R. Tedrake, Aggressive quadrotor flight through cluttered environments using mixed integer programming, in: *2016 IEEE international conference on robotics and automation (ICRA)*, IEEE, 2016, pp. 1469–1475.
- 725 [53] H. Oleynikova, M. Burri, Z. Taylor, J. Nieto, R. Siegwart, E. Galceran, Continuous-time trajectory optimization for online uav replanning, in: *2016 IEEE/RSJ International Conference on Intelligent Robots and Systems (IROS)*, IEEE, 2016, pp. 5332–5339.

- 730 [54] J. Chen, T. Liu, S. Shen, Online generation of collision-free trajectories for quadrotor flight in unknown cluttered environments, in: 2016 IEEE International Conference on Robotics and Automation (ICRA), IEEE, 2016, pp. 1476–1483.
- [55] R. Deits, R. Tedrake, Efficient mixed-integer planning for uavs in cluttered environments, in: 2015 IEEE international conference on robotics and automation (ICRA), IEEE, 2015, pp. 42–49.
- 735 [56] M. W. Mueller, M. Hehn, R. D’Andrea, A computationally efficient motion primitive for quadcopter trajectory generation, IEEE Transactions on Robotics 31 (6) (2015) 1294–1310.
- [57] P. Krüsi, B. Bücheler, F. Pomerleau, U. Schwesinger, R. Siegwart, P. Furgale, Lighting-invariant adaptive route following using iterative closest point matching, Journal of Field Robotics 32 (4) (2015) 534–564.
- 740 [58] S. J. Wright, Coordinate descent algorithms, Mathematical Programming 151 (1) (2015) 3–34.
- [59] J. Schulman, Y. Duan, J. Ho, A. Lee, I. Awwal, H. Bradlow, J. Pan, S. Patil, K. Goldberg, P. Abbeel, Motion planning with sequential convex optimization and convex collision checking, The International Journal of Robotics Research 33 (9) (2014) 1251–1270.
- 745 [60] Q.-C. Pham, A general, fast, and robust implementation of the time-optimal path parameterization algorithm, IEEE Transactions on Robotics 30 (6) (2014) 1533–1540.
- 750 [61] M. Pivtoraiko, D. Mellinger, V. Kumar, Incremental micro-uav motion replanning for exploring unknown environments, in: 2013 IEEE International Conference on Robotics and Automation, IEEE, 2013, pp. 2452–2458.
- [62] B. MacAllister, J. Butzke, A. Kushleyev, H. Pandey, M. Likhachev, Path planning for non-circular micro aerial vehicles in constrained environ-
- 755

- ments, in: 2013 IEEE International Conference on Robotics and Automation, IEEE, 2013, pp. 3933–3940.
- [63] M. Zucker, N. Ratliff, A. D. Dragan, M. Pivtoraiko, M. Klingensmith, C. M. Dellin, J. A. Bagnell, S. S. Srinivasa, Chomp: Covariant hamiltonian optimization for motion planning, *The International Journal of Robotics Research* 32 (9-10) (2013) 1164–1193.
- [64] D. Mellinger, A. Kushleyev, V. Kumar, Mixed-integer quadratic program trajectory generation for heterogeneous quadrotor teams, in: 2012 IEEE international conference on robotics and automation, IEEE, 2012, pp. 477–483.
- [65] S. Bhattacharya, M. Likhachev, V. Kumar, Topological constraints in search-based robot path planning, *Autonomous Robots* 33 (3) (2012) 273–290.
- [66] M. Kalakrishnan, S. Chitta, E. Theodorou, P. Pastor, S. Schaal, Stomp: Stochastic trajectory optimization for motion planning, in: 2011 IEEE international conference on robotics and automation, IEEE, 2011, pp. 4569–4574.
- [67] D. D. Harabor, A. Grastien, et al., Online graph pruning for pathfinding on grid maps., in: *AAAI*, 2011, pp. 1114–1119.
- [68] D. Lovi, N. Birkbeck, D. Cobzas, M. Jagersand, Incremental free-space carving for real-time 3d reconstruction, in: *Fifth international symposium on 3D data processing visualization and transmission (3DPVT)*, 2010.
- [69] N. Trawny, X. S. Zhou, K. Zhou, S. I. Roumeliotis, Interrobot transformations in 3-d, *IEEE Transactions on Robotics* 26 (2) (2010) 226–243.
- [70] M. W. Mehrez, G. K. Mann, R. G. Gosine, An optimization based approach for relative localization and relative tracking control in multi-robot systems, *Journal of Intelligent & Robotic Systems* 85 (2) (2017) 385–408.



- [71] G. Kulathunga, D. Devitt, A. Klimchik, Trajectory tracking for quadrotors: An optimization-based planning followed by controlling approach, *Journal of Field Robotics* 39 (7) (2022) 1003–1013.
- [72] M. J. Van Nieuwstadt, R. M. Murray, Real-time trajectory generation for differentially flat systems, *International Journal of Robust and Nonlinear Control: IFAC-Affiliated Journal* 8 (11) (1998) 995–1020.
- [73] C. Sferrazza, D. Pardo, J. Buchli, Numerical search for local (partial) differential flatness, in: *2016 IEEE/RSJ International Conference on Intelligent Robots and Systems (IROS)*, IEEE, 2016, pp. 3640–3646.
- [74] S. Krishnan, G. A. Rajagopalan, S. Kandhasamy, M. Shanmugavel, Towards scalable continuous-time trajectory optimization for multi-robot navigation, *arXiv preprint arXiv:1910.13463*.
- [75] D. Dolgov, S. Thrun, M. Montemerlo, J. Diebel, Path planning for autonomous vehicles in unknown semi-structured environments, *The International Journal of Robotics Research* 29 (5) (2010) 485–501.
- [76] P. Florence, J. Carter, R. Tedrake, Integrated perception and control at high speed: Evaluating collision avoidance maneuvers without maps, in: *Algorithmic Foundations of Robotics XII*, Springer, 2020, pp. 304–319.
- [77] B. T. Lopez, J. P. How, Aggressive 3-d collision avoidance for high-speed navigation., in: *ICRA, 2017*, pp. 5759–5765.
- [78] W. J. Gordon, R. F. Riesenfeld, B-spline curves and surfaces, in: *Computer aided geometric design*, Elsevier, 1974, pp. 95–126.
- [79] J. A. Sethian, *Level set methods and fast marching methods: evolving interfaces in computational geometry, fluid mechanics, computer vision, and materials science*, Vol. 3, Cambridge university press, 1999.
- [80] P. Sava, S. Fomel, 3-d traveltime computation using Huygens wavefront tracing, *Geophysics* 66 (3) (2001) 883–889.

- 810 [81] S. M. LaValle, Planning algorithms, Cambridge university press, 2006.
- [82] K. Bergman, O. Ljungqvist, T. Glad, D. Axehill, An optimization-based receding horizon trajectory planning algorithm, arXiv preprint arXiv:1912.05259.
- [83] J. D. Head, M. C. Zerner, A broyden—fletcher—goldfarb—shanno optimization procedure for molecular geometries, Chemical physics letters  
815 122 (3) (1985) 264–270.
- [84] C. de Boor, Subroutine package for calculating with b-splines, Los Alamos Scient. Lab. Report LA-4728-MS.
- [85] K. Qin, General matrix representations for b-splines, The Visual Computer 16 (3-4) (2000) 177–186.  
820
- [86] J. Hu, Z. Ma, Y. Niu, W. Tian, W. Yao, Real-time trajectory replanning for quadrotor using octomap and uniform b-splines, in: International Conference on Intelligent Robotics and Applications, Springer, 2019, pp. 727–741.
- 825 [87] M. E. Flores Contreras, Real-time trajectory generation for constrained nonlinear dynamical systems using non-uniform rational b-spline basis functions, Ph.D. thesis, California Institute of Technology (2008).
- [88] J. A. Preiss, W. Hönig, N. Ayanian, G. S. Sukhatme, Downwash-aware trajectory planning for large quadrotor teams, in: 2017 IEEE/RSJ International Conference on Intelligent Robots and Systems (IROS), IEEE,  
830 2017, pp. 250–257.
- [89] A. Hornung, K. M. Wurm, M. Bennewitz, C. Stachniss, W. Burgard, Octomap: An efficient probabilistic 3d mapping framework based on octrees, Autonomous robots 34 (3) (2013) 189–206.
- 835 [90] R. Kala, Rapidly exploring random graphs: motion planning of multiple mobile robots, Advanced Robotics 27 (14) (2013) 1113–1122.

- [91] Z. Zhu, E. Schmerling, M. Pavone, A convex optimization approach to smooth trajectories for motion planning with car-like robots, in: 2015 54th IEEE Conference on Decision and Control (CDC), IEEE, 2015, pp. 835–842.
- [92] S. Quinlan, O. Khatib, Elastic bands: Connecting path planning and control, in: [1993] Proceedings IEEE International Conference on Robotics and Automation, IEEE, 1993, pp. 802–807.
- [93] D. Jacobson, D. Mayne, Differential dynamic programming elsevier new york (1970).
- [94] E. Theodorou, D. Krishnamurthy, E. Todorov, From information theoretic dualities to path integral and kullback-leibler control: Continuous and discrete time formulations, in: The Sixteenth Yale Workshop on Adaptive and Learning Systems, 2013.
- [95] F. L. Lewis, V. L. Syrmos, Optimal control, john-wiley&sons, New York.
- [96] W. Sun, J. Van Den Berg, R. Alterovitz, Stochastic extended lqr: Optimization-based motion planning under uncertainty, in: Algorithmic Foundations of Robotics XI, Springer, 2015, pp. 609–626.
- [97] J. Van Den Berg, D. Wilkie, S. J. Guy, M. Niethammer, D. Manocha, Lqg-obstacles: Feedback control with collision avoidance for mobile robots with motion and sensing uncertainty, in: 2012 IEEE International Conference on Robotics and Automation, IEEE, 2012, pp. 346–353.
- [98] M. Likhachev, G. J. Gordon, S. Thrun, Ara\*: Anytime a\* with provable bounds on sub-optimality, in: Advances in neural information processing systems, 2004, pp. 767–774.
- [99] S. Karaman, E. Frazzoli, Sampling-based algorithms for optimal motion planning, The international journal of robotics research 30 (7) (2011) 846–894.

- [100] A. Perez, R. Platt, G. Konidaris, L. Kaelbling, T. Lozano-Perez, Lqr-  
rrt\*: Optimal sampling-based motion planning with automatically derived  
865 extension heuristics, in: 2012 IEEE International Conference on Robotics  
and Automation, IEEE, 2012, pp. 2537–2542.
- [101] G. Kulathunga, D. Devitt, R. Fedorenko, A. Klimchik, Path planning  
followed by kinodynamic smoothing for multirotor aerial vehicles (mavs),  
870 Russian Journal of Nonlinear Dynamics 17 (4) (2021) 491–505.
- [102] V. Pacelli, O. Arslan, D. E. Koditschek, Integration of local geometry and  
metric information in sampling-based motion planning, in: 2018 IEEE  
International Conference on Robotics and Automation (ICRA), IEEE,  
2018, pp. 3061–3068.
- 875 [103] M. T. Mason, J. K. Salisbury Jr, Robot hands and the mechanics of  
manipulation, The MIT Press, Cambridge, MA, 1985.
- [104] S. Liu, N. Atanasov, K. Mohta, V. Kumar, Search-based motion plan-  
ning for quadrotors using linear quadratic minimum time control, in:  
2017 IEEE/RSJ international conference on intelligent robots and sys-  
880 tems (IROS), IEEE, 2017, pp. 2872–2879.
- [105] A. D. Ames, K. Galloway, K. Sreenath, J. W. Grizzle, Rapidly exponen-  
tially stabilizing control lyapunov functions and hybrid zero dynamics,  
IEEE Transactions on Automatic Control 59 (4) (2014) 876–891.
- [106] G. Wu, K. Sreenath, Safety-critical and constrained geometric control  
885 synthesis using control lyapunov and control barrier functions for systems  
evolving on manifolds, in: 2015 American Control Conference (ACC),  
IEEE, 2015, pp. 2038–2044.
- [107] I. Kolmanovsky, E. Garone, S. Di Cairano, Reference and command gov-  
ernors: A tutorial on their theory and automotive applications, in: 2014  
890 American Control Conference, IEEE, 2014, pp. 226–241.

- [108] E. Garone, M. M. Nicotra, Explicit reference governor for constrained nonlinear systems, *IEEE Transactions on Automatic Control* 61 (5) (2015) 1379–1384.
- [109] O. Arslan, D. E. Koditschek, Smooth extensions of feedback motion planners via reference governors, in: 2017 IEEE International Conference on Robotics and Automation (ICRA), IEEE, 2017, pp. 4414–4421.
- [110] Z. Li, O. Arslan, N. Atanasov, Fast and safe path-following control using a state-dependent directional metric, *arXiv preprint arXiv:2002.02038*.
- [111] Y. Aoyama, G. Boutselis, A. Patel, E. A. Theodorou, Constrained differential dynamic programming revisited (2020). *arXiv:arXiv:2005.00985*.
- [112] C. Liu, J. Pan, Y. Chang, Pid and lqr trajectory tracking control for an unmanned quadrotor helicopter: Experimental studies, in: 2016 35th Chinese Control Conference (CCC), IEEE, 2016, pp. 10845–10850.
- [113] I. D. Cowling, J. F. Whidborne, A. K. Cooke, Optimal trajectory planning and lqr control for a quadrotor uav, in: International Conference on Control, 2006.
- [114] M. Bangura, R. Mahony, Real-time model predictive control for quadrotors, *IFAC Proceedings Volumes* 47 (3) (2014) 11773 – 11780, 19th IFAC World Congress. doi:<https://doi.org/10.3182/20140824-6-ZA-1003.00203>.  
URL <http://www.sciencedirect.com/science/article/pii/S1474667016434890>
- [115] T. Ohtsuka, H. A. Fujii, Real-time optimization algorithm for nonlinear receding-horizon control, *Automatica* 33 (6) (1997) 1147–1154.
- [116] H. Deng, T. Ohtsuka, A parallel newton-type method for nonlinear model predictive control, *Automatica* 109 (2019) 108560.

- [117] I. S. Mohamed, G. Allibert, P. Martinet, Model predictive path integral control framework for partially observable navigation: A quadrotor case study, arXiv preprint arXiv:2004.08641.
- 920 [118] M. A. Olivares-Mendez, P. Campoy, I. Mellado-Bataller, L. Mejias, See-and-avoid quadcopter using fuzzy control optimized by cross-entropy, in: 2012 IEEE International Conference on Fuzzy Systems, Ieee, 2012, pp. 1–7.
- [119] J. Tordesillas, B. T. Lopez, M. Everett, J. P. How, Faster: Fast and safe trajectory planner for flights in unknown environments, arXiv preprint  
925 arXiv:2001.04420.
- [120] S. Quinlan, Real-time modification of collision-free paths, no. 1537, Stanford University Stanford, 1994.
- [121] B. Zhou, F. Gao, J. Pan, S. Shen, Robust real-time uav replanning using  
930 guided gradient-based optimization and topological paths, in: 2020 IEEE International Conference on Robotics and Automation (ICRA), IEEE, 2020, pp. 1208–1214.
- [122] M. J. Powell, The bobyqa algorithm for bound constrained optimization without derivatives, Cambridge NA Report NA2009/06, University  
935 of Cambridge, Cambridge (2009) 26–46.
- [123] D. C. Liu, J. Nocedal, On the limited memory bfgs method for large scale optimization, *Mathematical programming* 45 (1-3) (1989) 503–528.
- [124] B. Houska, H. J. Ferreau, M. Diehl, Acado toolkit—an open-source framework for automatic control and dynamic optimization, *Optimal Control  
940 Applications and Methods* 32 (3) (2011) 298–312.
- [125] D. Kraft, A software package for sequential quadratic programming. forschungsbericht-deutsche forschungs-und versuchsanstalt fur luft-und raumfahrt, DFVLR, Köln.

- [126] N. Parikh, S. Boyd, Block splitting for distributed optimization, *Mathematical Programming Computation* 6 (1) (2014) 77–102.
- [127] C. Fougner, S. Boyd, Parameter selection and preconditioning for a graph form solver, in: *Emerging Applications of Control and Systems Theory*, Springer, 2018, pp. 41–61.
- [128] K. Svanberg, A class of globally convergent optimization methods based on conservative convex separable approximations, *SIAM journal on optimization* 12 (2) (2002) 555–573.
- [129] X. Liu, R. D. Wiersma, Optimization based trajectory planning for real-time 6dof robotic patient motion compensation systems, *PloS one* 14 (1) (2019) e0210385.
- [130] P. Foehn, D. Falanga, N. Kuppaswamy, R. Tedrake, D. Scaramuzza, Fast trajectory optimization for agile quadrotor maneuvers with a cable-suspended payload.
- [131] M. Geisert, N. Mansard, Trajectory generation for quadrotor based systems using numerical optimal control, in: *2016 IEEE international conference on robotics and automation (ICRA)*, IEEE, 2016, pp. 2958–2964.
- [132] S. Shen, N. Michael, V. Kumar, Stochastic differential equation-based exploration algorithm for autonomous indoor 3d exploration with a micro-aerial vehicle, *The International Journal of Robotics Research* 31 (12) (2012) 1431–1444.
- [133] S. G. Johnson, The nlopt nonlinear-optimization package, 2014, URL <http://ab-initio.mit.edu/nlopt>.
- [134] X. Zhou, Z. Wang, H. Ye, C. Xu, F. Gao, Ego-planner: An esdf-free gradient-based local planner for quadrotors, *IEEE Robotics and Automation Letters*.

- 970 [135] R. D. T. STEiha, Truncatednewton algorithmsforlarge-scale optimization, *Math. Programming* 26 (1983) 190–212.
- [136] E. D. Andersen, K. D. Andersen, The mosek interior point optimizer for linear programming: an implementation of the homogeneous algorithm, in: *High performance optimization*, Springer, 2000, pp. 197–232.
- 975 [137] I. Gurobi Optimization, Gurobi optimizer reference manual (2018).
- [138] B. Stellato, G. Banjac, P. Goulart, A. Bemporad, S. Boyd, Osqp: An operator splitting solver for quadratic programs, *Mathematical Programming Computation* (2020) 1–36.
- [139] M. Kamel, T. Stastny, K. Alexis, R. Siegwart, Model predictive control  
980 for trajectory tracking of unmanned aerial vehicles using robot operating system, in: *Robot operating system (ROS)*, Springer, 2017, pp. 3–39.
- [140] E. M. Gertz, S. J. Wright, Object-oriented software for quadratic programming, *ACM Transactions on Mathematical Software (TOMS)* 29 (1) (2003) 58–81.
- 985 [141] J. Tordesillas, J. P. How, Mader: Trajectory planner in multi-agent and dynamic environments, arXiv preprint arXiv:2010.11061.
- [142] J. Tordesillas, J. P. How, Minvo basis: Finding simplexes with minimum volume enclosing polynomial curves, arXiv preprint arXiv:2010.10726.
- [143] A. R. Conn, N. I. Gould, P. Toint, A globally convergent augmented  
990 lagrangian algorithm for optimization with general constraints and simple bounds, *SIAM Journal on Numerical Analysis* 28 (2) (1991) 545–572.
- [144] L. Tang, H. Wang, P. Li, Y. Wang, Real-time trajectory generation for quadrotors using b-spline based non-uniform kinodynamic search, in: *2019 IEEE International Conference on Robotics and Biomimetics (ROBIO)*,  
995 IEEE, 2019, pp. 1133–1138.



- [145] J. A. Andersson, J. Gillis, G. Horn, J. B. Rawlings, M. Diehl, Casadi: a software framework for nonlinear optimization and optimal control, *Mathematical Programming Computation* 11 (1) (2019) 1–36.
- [146] L. T. Biegler, V. M. Zavala, Large-scale nonlinear programming using ipopt: An integrating framework for enterprise-wide dynamic optimization, *Computers & Chemical Engineering* 33 (3) (2009) 575–582.